5-hydroxytryptamine synthesized in the aorta-gonad-mesonephros regulates hematopoietic stem and progenitor cell survival

Junhua Lv,[1,2]* Lu Wang,[1]* Ya Gao,[1] Yu-Qiang Ding,[3] and Feng Liu[1,2]

[1]State Key Laboratory of Membrane Biology, Institute of Zoology, Chinese Academy of Sciences, Beijing 100101, China
[2]University of Chinese Academy of Sciences, Beijing 100049, China
[3]Key Laboratory of Arrhythmias, Ministry of Education, East Hospital, Department of Anatomy and Neurobiology, Collaborative Innovation Center for Brain Science, Tongji University School of Medicine, Shanghai 200092, China

The in vitro or ex vivo production of transplantable hematopoietic stem cells (HSCs) holds great promise for the treatment of hematological diseases in the clinic. However, HSCs have not been produced from either embryonic or induced pluripotent stem cells. In this study, we report that 5-hydroxytryptamine (5-HT; also called serotonin) can enhance the generation of hematopoietic stem and progenitor cells (HSPCs) in vitro and is essential for the survival of HSPCs in vivo during embryogenesis. In *tryptophan hydroxylase 2*–deficient embryos, a decrease in 5-HT synthesized in the aorta-gonad-mesonephros leads to apoptosis of nascent HSPCs. Mechanistically, 5-HT inhibits the AKT-Foxo1 signaling cascade to protect the earliest HSPCs in intraaortic hematopoietic clusters from excessive apoptosis. Collectively, our results reveal an unexpected role of 5-HT in HSPC development and suggest that 5-HT signaling may be a potential therapeutic target for promoting HSPC survival.

INTRODUCTION

Hematopoietic stem cells (HSCs) possess the capacity to produce >10 different functional specialized cell lineages, as well as the ability to self-renew. The clinical use of HSC transplantation to treat hematological diseases makes it extraordinarily important to obtain a sufficient number of transplantable HSCs. Statistical data presented in 2010 showed that >50,000 patients suffering from hematological diseases and other malignancies require HSC transplantation every year (Gratwohl et al., 2010). The demand for functional HSCs is rapidly increasing, and great efforts have been spent to try to obtain large numbers of HSCs for potential transplantation.

Recently, progress has been made in expanding umbilical cord blood-derived hematopoietic stem and progenitor cells (HSPCs). The small molecule SR1 and RNA binding protein Musashi2 could both directly suppress the expression of aryl hydrocarbon receptor and promote the expansion of cord blood HSPCs that retain multilineage capacity and are capable of long-term engraftment (Boitano et al., 2010; Rentas et al., 2016). UM171, another small molecule, has been used for the ex vivo expansion of human HSPCs, demonstrating the ability to reconstitute the blood system of immunodeficient mice for >6 mo; UM171 also enhances the self-renewal of HSPCs by suppressing transcripts associated with differentiation (Fares et al., 2014). Engineered Notch ligand (Delta1$^{ext\text{-}IgG}$) stimulates the ex vivo expansion of human CD34$^+$ cord blood cells and enhances their repopulation ability in immunodeficient nonobese diabetic (NOD)/SCID mice (Delaney et al., 2010).

It has been well documented that the earliest HSCs arise from a specialized endothelial population, known as the hemogenic endothelium (HE), through the endothelial-to-hematopoietic transition in the ventral wall of the dorsal aorta (DA) of mouse and zebrafish embryos (Zovein et al., 2008; Bertrand et al., 2010; Boisset and Robin, 2010; Kissa and Herbomel, 2010). Once they have formed in the aorta-gonad-mesonephros (AGM) region from embryonic day 10.5 (E10.5) and E12.5 in mice, HSPCs migrate to and expand in the fetal liver before colonizing the bone marrow before birth (Kumaravelu et al., 2002; Orkin and Zon, 2008). Despite decades of efforts, the extrinsic and intrinsic regulatory factors controlling HSPC development remain incompletely understood.

Previous studies reported a functional link between the development of HSPCs and the nervous system. For instance, *gata3* deficiency impairs HSPC development by controlling the production of catecholamine in cells of the sympathetic

*J. Lv and L. Wang contributed equally to this paper.

Correspondence to Feng Liu: liuf@ioz.ac.cn

Abbreviations used: 5-HT, 5-hydroxytryptamine; AAAD, aromatic amino acid decarboxylase; AGM, aorta-gonad-mesonephros; CFU-C, CFUs in the culture; CNS, central nervous system; DA, dorsal aorta; DEG, differentially expressed gene; ee, embryo equivalent; GO, gene ontology; HE, hemogenic endothelium; HSC, hematopoietic stem cell; HSPC, hematopoietic stem and progenitor cell; IAHC, intraaortic hematopoietic cluster; LC-MS, liquid chromatography–mass spectrometry; MT, methoxytryptamine; qPCR, quantitative real-time PCR; Shh, sonic hedgehog; sp, somite pairs; TPH, tryptophan hydroxylase.

The Rockefeller University Press $30.00
J. Exp. Med. 2017 Vol. 214 No. 2 529–545
https://doi.org/10.1084/jem.20150906

Supplemental material can be found at:
http://doi.org/10.1084/jem.20150906

nervous system (Fitch et al., 2012). Our previous study also showed that Fev, also known as Pet1 in mammals, is an important regulator of HSPC development in zebrafish and humans (Wang et al., 2013). The well-known role of Pet1 is to regulate the synthesis of 5-hydroxytryptamine (5-HT), and *pet1* deficiency leads to the inhibition of the differentiation of the majority of 5-HT–producing neurons and a 70–80% decrease in 5-HT (Hendricks et al., 2003; Lillesaar et al., 2007). Interestingly, the addition of 5-HT can promote the expansion of human cord blood $CD34^+$ cells and increase their hematopoietic repopulating ability in NOD/SCID mice (Yang et al., 2007). Therefore, the regulatory effects of Pet1 on 5-HT synthesis and the expansion of human cord blood $CD34^+$ cells by 5-HT prompted us to propose that 5-HT might be involved in HSPC development during vertebrate embryogenesis.

5-HT is a monoamine neurotransmitter or hormone that is secreted from both the central nervous system (CNS) and peripheral nervous system to regulate behaviors. 5-HT has been shown to be related to feelings of well-being and happiness (Liu et al., 2014; Li et al., 2016). The primary sources of 5-HT release are the raphe nucleus in the brain and the gastrointestinal tract (Ben Arous et al., 2009). In animals, including humans, 5-HT is synthesized from the amino acid L-tryptophan by two enzymes: tryptophan hydroxylase (Tph) and aromatic amino acid decarboxylase (AAAD). The Tph-mediated reaction is the rate-limiting step in 5-HT synthesis (Lovenberg et al., 1967; Ichiyama et al., 1970). Tph has two forms: Tph1 and Tph2 (Côté et al., 2003). Tph1 is mostly expressed in peripheral tissues, such as the skin, gut, and pineal gland, but is also expressed in the CNS (Zill et al., 2009). Tph2 is the predominant isoform in the CNS. AAAD catalyzes several different decarboxylation reactions, such as 5-HTP to 5-HT, L-DOPA to dopamine, and others (Christie et al., 2014). 5-HT functions through its receptors on the cell membrane of nerve cells and other cell types to activate the intracellular second messenger cascade (Hannon and Hoyer, 2008). To date, it has not yet been reported whether 5-HT or its receptors can directly regulate HSPC development during embryogenesis.

In this study, we show that 5-HT, which is synthesized in the AGM, acts as a novel endogenous regulator of HSPC development and promotes the survival of HSPCs in the intraaortic hematopoietic cluster (IAHC). Mechanistically, the effect of 5-HT on HSPC development is mainly mediated through Htr5a by inhibiting the proapoptotic pathway.

RESULTS

5-HT promotes the generation of HSPCs in vitro and ex vivo

Although 5-HT treatment could expand $CD34^+$ cord blood cells in vitro and increase the number of repopulating $CD45^+$ cells in the bone marrow of the recipients (Yang et al., 2007), the mechanism of 5-HT regulating this process and its role during embryogenesis remain unknown. Different chemicals were used in an AGM explant culture system to explore the effect of 5-HT on HSPC expansion at embryonic stages. In brief, the AGMs were dissected from wild-type embryos at E10.0–E10.5 (31–40 somite pairs [sp]) and cultured on Durapore filters, which were placed at the air–liquid interface, in the presence of 5-HT, fluoxetine, or methoxytryptamine (MT). After treatment for 36–48 h, the AGMs were subjected to further analysis (Fig. 1 A). 5-HT treatment increased the colony numbers in the CFUs in the culture (CFU-C) assay, including burst forming unit–erythroid (BFU-E), CFU-granulomonocyte (CFU-GM), and CFU-mix (Fig. 1 B). Because *runx1* and *gfi1* are both highly expressed in the IAHC and play pivotal roles in HSPC development (Chen et al., 2009; Thambyrajah et al., 2016), the mRNA levels of *runx1* and *gfi1* were examined, and the results showed that their expression was up-regulated (Fig. 1 C). Most of the 5-HT in the intercellular space can be reabsorbed by the 5-HT transporter. Fluoxetine is a selective serotonin reuptake inhibitor and can also inhibit the reabsorption of the remaining 5-HT in the peripheral tissues (Wong et al., 1974; Ortiz and Artigas, 1992; Bianchi et al., 2002). Fluoxetine treatment also increased the number of spleen colonies in irradiated adult recipients (Fig. 1 D), as well as the expression of *runx1* and *gfi1* (Fig. 1 E). In contrast, the administration of MT, a competitive inhibitor of 5-HT, had the opposite effects (Fig. 1, F and G). Collectively, these chemical treatment data indicate that 5-HT promotes the generation of HSPCs in vitro and ex vivo.

The development of HSPCs is impaired in 5-HT–deficient mouse embryos

5-HT synthesis is regulated by complex signaling pathways and transcription factors during embryogenesis, and the Tph-mediated reaction is the rate-limiting step in this process (Fig. 2 A; Lovenberg et al., 1967; Ichiyama et al., 1970; Ding et al., 2003). AGMs from E10.5 and E11.0 $tph2^{+/+}$ and $tph2^{+/-}$ embryos were used to investigate whether 5-HT plays a role in HSPC development during embryogenesis. Strikingly, staining with an anti-Runx1 antibody showed an apparent reduction in Runx1 expression in the AGM of $tph2^{+/-}$ embryos (Fig. 2 B). Although hematopoietic clusters formed on the ventral wall of the DA, the size and number of clusters in $tph2^{+/-}$ embryos were significantly reduced compared with control embryos (Fig. 2, B and C). Similarly, the mRNA levels of *runx1* and *gfi1* were significantly decreased in the $tph2^{+/-}$ AGM (Fig. 2 D). Flow cytometry analysis showed that the number of c-kit^+CD34^+ cells (HSPCs) was decreased by ∼80% in the AGM of $tph2^{+/-}$ embryos at E11.5 (Fig. 2 E), whereas there was no obvious change in c-kit^+CD31^+ cells (HE cells) at E10.5 (Fig. 2 F). In addition, analysis of the peripheral blood showed that there was an apparent decrease in the ratio of definitive, enucleated erythrocytes (EryD) to primitive, nucleated erythroblasts (EryP) in the fetal liver of $tph2^{+/-}$ embryos at E14.5 (Fig. 2 G), suggesting that definitive hematopoiesis was attenuated in $tph2^{+/-}$ embryos.

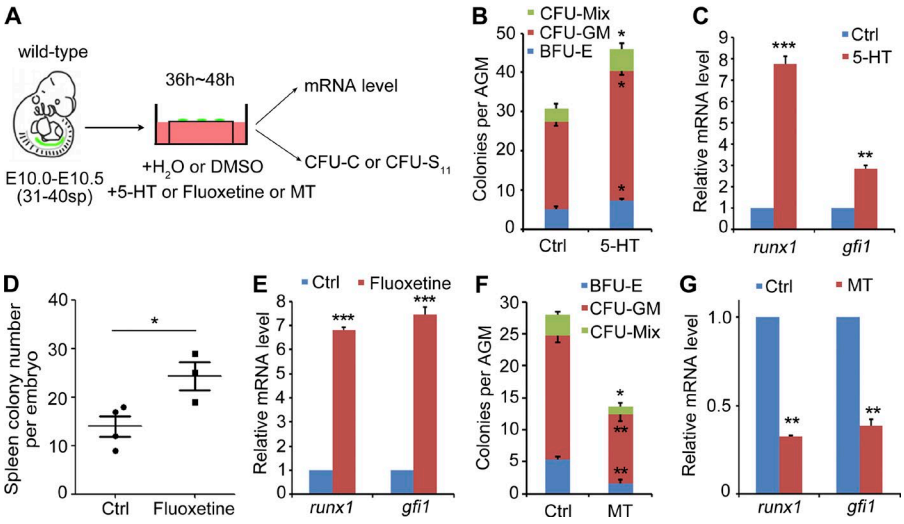

Figure 1. **5-HT promotes the development of HSPCs in vitro and ex vivo.** (A) Flow chart of using different chemicals to detect the requirement of 5-HT for HSPCs production by an AGM explants culture system. In brief, E10.0–E10.5 embryo (31–40 sp) AGMs were dissected from the wild-type embryos and cultured on Durapore filters at the air–liquid interface in the presence of 5-HT, fluoxetine, or MT diluted in M5300 long-term culture medium. After 36–48 h, AGMs were used to quantify the mRNA level of hematopoietic related genes (*runx1* and *gfi1*). The remaining AGMs were dissociated with collagenase and used for CFU-C or CFU-S_{11} assay. (B) CFU-C assay of AGMs treated with 5-HT at 1 mM. 1 ee was used. (C) qPCR analysis showed the expression of *runx1* and *gfi1* in the AGM treated with 5-HT. (D) CFU-S_{11} assay with AGMs treated with fluoxetine at 10 µM. The number of spleen colonies in irradiated adult recipients were counted. 1 ee was used. (E) qPCR analysis showed the expression of *runx1* and *gfi1* in the AGM treated with fluoxetine. (F) CFU-C assay of AGMs treated with MT at 50 µM. 1 ee was used. (G) qPCR analysis showed the expression of *runx1* and *gfi1* in the AGM treated with MT. The results are presented as mean ± SE. Student's *t* test: *, $P < 0.05$; **, $P < 0.01$; ***, $P < 0.001$. $n = 3$. BFU-E, burst forming unit–erythroid; CFU-GM, CFU-granulomonocyte; Ctrl, control.

We further examined the hematopoietic phenotype in *pet1*-cre;*tph2*$^{+/fl}$ and *vec*-cre;*tph2*$^{+/fl}$ embryos to confirm the impairments in definitive hematopoiesis in the *tph2*$^{+/-}$ embryos (Kriegebaum et al., 2010). Immunofluorescence analysis showed an apparent reduction in Runx1 expression (Fig. 2 H), and the size and number of hematopoietic clusters were also markedly reduced in *pet1*-cre;*tph2*$^{+/fl}$ embryos (Fig. 2, H and I). Moreover, the formation of hematopoietic clusters was obviously suppressed in *vec*-cre;*tph2*$^{+/fl}$ embryos at E10.5 and E11.0 (Fig. 2, J–L). This further confirms that the decrease of *tph2* in endothelial cells can affect the development of HSPCs in IAHCs. We next characterized the function of HSPCs in *tph2*$^{+/-}$ embryos. The CFU-spleen (CFU-S_{11}) assay and long-term transplantation showed that the reconstitution ability of HSPCs from *tph2*$^{+/-}$ embryos was significantly compromised, possibly because of the decrease in 5-HT levels (Fig. 2, M and N). Overall, these data showed that *tph2* expressed in endothelial cells of the AGM is important for HSPC development during embryogenesis in mice.

AKT-Foxo1–mediated apoptotic signaling suppresses HSPC survival in *tph2* haploinsufficient embryos

An mRNA sequencing (mRNA-Seq) analysis was performed using the AGMs of *tph2*$^{+/+}$ and *tph2*$^{+/-}$ embryos to understand the impairments in definitive hematopoiesis in *tph2*$^{+/-}$ embryos at the molecular level. Heat map analysis revealed several differentially expressed genes (DEGs) between the two groups (Fig. 3 A), and an expanded gene list is provided in Table S2. Gene ontology (GO) analysis revealed that a set of down-regulated genes in the *tph2*$^{+/-}$ embryos was enriched in neurogenesis, which validated the decrease in the 5-HT levels, as well as the sequencing quality. In addition, the genes that were markedly down-regulated in the *tph2*$^{+/-}$ embryos were enriched in PI3K–AKT signaling. Meanwhile, some genes that were up-regulated in the *tph2*$^{+/-}$ embryos were enriched in the cell apoptotic process (Fig. 3 B). PI3K–AKT signaling is a well-known pathway involved in cell survival (Song et al., 2005). Our results are also consistent with previous studies showing that 5-HT exerted antiapoptotic effects in red blood cells and M-07e cells, a megakaryoblastic cell line (Yang et al., 2007; Amireault et al., 2011).

Based on the RNA-Seq data and previous studies (Yang et al., 2007; Amireault et al., 2011), cell apoptosis was investigated by staining E10.5 *tph2*$^{+/-}$ embryos with an anti–cleaved caspase3 (cCasp3) antibody. As expected, the CD31^{+}CD34^{+} cells in the IAHC tended to be apoptotic, and the number of cCasp3, CD31, and CD34 costained cells in each embryo was significantly increased in *tph2*$^{+/-}$ embryos (Fig. 3 C). A TUNEL (terminal deoxynucleotidyl transferase deoxyuridine triphosphate nick-end labeling) assay further demonstrated the apoptotic nature of CD31^{+}Runx1^{+} cells in the IAHC (Fig. 3 D). In accordance with the results observed for *tph2*$^{+/-}$ embryos, the staining in *pet1*-cre;*tph2*$^{+/fl}$ and *vec*-cre;*tph2*$^{+/fl}$ embryos showed similar results (Fig. 3, E and F). These results showed that the HSPCs in the IAHC tended to be apoptotic in *tph2* haploinsufficient embryos, which supports the observation that the number and size of the IAHCs (Fig. 2, B and C) and the number of c-kit^{+}CD34^{+} cells in *tph2*$^{+/-}$ embryos (Fig. 2 E) were decreased.

Next, immunofluorescence and Western blot analyses showed that the levels of phosphorylated AKT (pAKT) were decreased, which was mainly restricted to the endothelial cells and mesenchymal cells in the AGM (Fig. 3, G and H). AKT inhibitor IV and an AKT activator, Fumonisin B1, were used

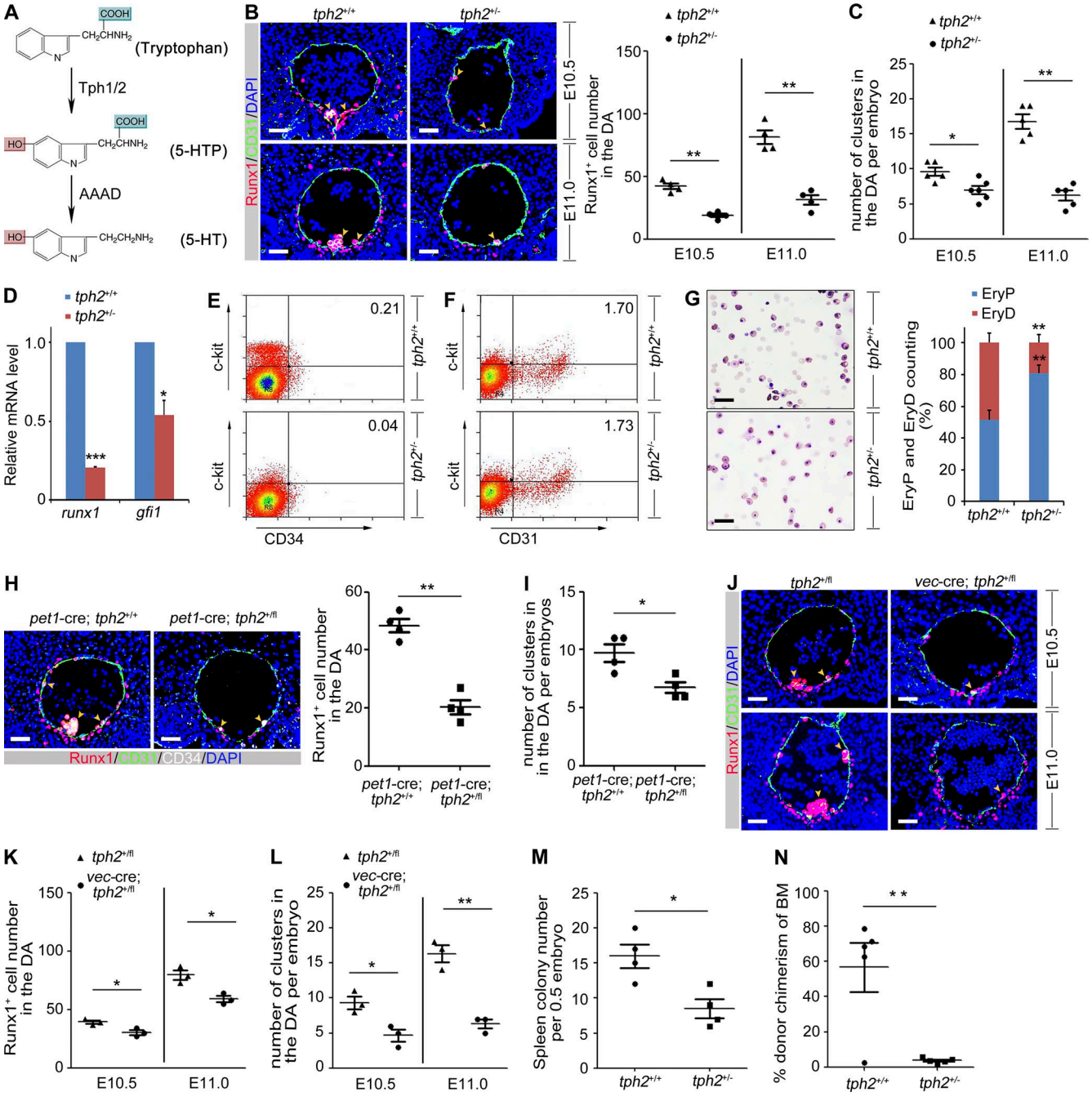

Figure 2. **The development of HSPCs is impaired in 5-HT–deficient mouse embryos.** (A) Flow chart of 5-HT synthesized from tryptophan by Tph1/2 and AAAD. (B) Immunofluorescence analysis on sections of *tph2*$^{+/+}$ and *tph2*$^{+/-}$ embryos at E10.5 and E11.0 with anti-Runx1 and anti-CD31 antibodies. IAHC is marked with yellow arrowheads. (Right) Quantification of Runx1-positive cells in the DA of the sections. Bars, 10 µm. $n \geq 4$. (C) Quantification of hematopoietic clusters (yellow arrowheads shown in B) in the DA of *tph2*$^{+/+}$ and *tph2*$^{+/-}$ embryos at E10.5 and E11.0. $n \geq 4$. (D) qPCR analysis showed the mRNA levels of *runx1* and *gfi1* in the AGM of *tph2*$^{+/-}$ embryos compared with the controls. $n = 3$. (E) Flow cytometry results showing the percentage of c-kit$^+$ CD34$^+$ cells in the AGM of *tph2*$^{+/-}$ embryos at E11.5. (F) Flow cytometry results showing the percentage of c-Kit$^+$ CD31$^+$ cells in the AGM of *tph2*$^{+/-}$ embryos at E10.5 compared with the control. (G) Peripheral blood analysis showing the ratio of definitive, enucleated erythrocytes (EryD) to primitive, nucleated erythroblasts (EryP) in *tph2*$^{+/+}$ and *tph2*$^{+/-}$ embryos at E14.5. Bars, 10 µm. $n = 3$. (H, left) Immunofluorescence analysis on sections of *pet1*-cre;*tph2*$^{+/+}$ and *pet1*-cre;*tph2*$^{+/fl}$ embryos at E10.5 with anti-CD31, anti-CD34, and anti-Runx1 antibodies. IAHC is marked with yellow arrowheads. (Right) Quantification of Runx1-positive cells in the DA of the sections. Bars, 10 µm. $n = 4$. (I) Quantification of hematopoietic clusters (yellow arrowhead shown in H [left]) in the DA of *pet1*-cre;*tph2*$^{+/+}$ and *pet1*-cre;*tph2*$^{+/fl}$ embryos at E10.5. $n = 4$. (J) Immunofluorescence analysis on sections of *tph2*$^{+/fl}$ and *vec*-cre;*tph2*$^{+/fl}$ embryos at E10.5 and E11.0 with anti-CD31 and anti-Runx1 antibodies. IAHC is marked with yellow arrowhead. Bars, 10 µm. (K) Quantification of Runx1-positive cells

in the AGM explant culture to determine whether decreased PI3K–AKT signaling was responsible for the impairments in definitive hematopoiesis observed in *tph2*$^{+/-}$ embryos. First, AKT inhibitor IV decreased the level of pAKT, whereas the AKT activator increased the pAKT levels (not depicted). Importantly, the addition of AKT inhibitor IV decreased the colony numbers in the CFU-C assay (Fig. 3 I) and decreased the expression of *runx1* and *gfi1* (Fig. 3 J). Second, treatment with Fumonisin B1 exerted opposite effects on hematopoiesis (Fig. 3, K and L). These data confirmed an important role for the AKT pathway, which is downstream of 5-HT signaling, in HSPC development.

Forkhead box protein O1 (Foxo1) can be phosphorylated by AKT signaling and then inhibit the transcription of target genes (Rena et al., 1999); Foxo1 also plays important roles in apoptosis, cell cycle arrest, and the stress response (Eijkelenboom and Burgering, 2013). Foxo1 is localized in the nucleus to activate its downstream targets, such as the proapoptotic genes *bim* and *fasl*, and its transcriptional activity is dependent on its phosphorylation state. In *tph2*$^{+/-}$ embryos, an obvious decrease in phosphorylated Foxo1 (pFoxo1) and increase in Foxo1 were observed in the AGM (Fig. 3 M), and these changes in pFoxo1 and Foxo1 were mainly observed in endothelial cells and mesenchymal cells (Fig. 3 N). It has been reported that *bim* and *fasl* are both proapoptotic genes that can be directly regulated by Foxo1 (Raghavendra et al., 2009; Shukla et al., 2014). Our data also showed that *bim* and *fasl* were both up-regulated in the AGM of *tph2*$^{+/-}$ embryos (Fig. 3 O). Quantitative real-time PCR (qPCR) analysis was performed using AGMs that had been treated with different chemicals to further investigate the regulation of *bim* and *fasl* by the 5-HT–AKT-Foxo1 cascade. Treatment with 5-HT, fluoxetine, and Fumonisin B1 inhibited the transcription of *bim* and *fasl*, whereas treatment with the AKT inhibitor increased their transcription (Fig. 3, P and Q). The CFU-C assay showed that AKT activation efficiently rescued the decreased colony number and *runx1* and *gfi1* expression in *tph2*$^{+/-}$ embryos (Fig. 3, R and S). Together, these in vivo and in vitro data support the hypothesis that up-regulated activity of the proapoptotic pathway leads to the impaired survival of HSPCs in *tph2* haploinsufficient embryos.

5-HT is biosynthesized in the AGM to regulate definitive hematopoiesis

Pet1 is tightly controlled by sonic hedgehog (Shh) signaling and the Nkx2-2–Lmx1b cascade to regulate 5-HT production during development (Fig. 4 A; Ding et al., 2003). We first analyzed the expression pattern of Pet1 to determine whether 5-HT from the CNS or peripheral tissues regulates definitive hematopoiesis in mice. Consistent with its expression in the AGM in zebrafish (Wang et al., 2013), Pet1 was also expressed in hematopoietic cluster cells, endothelial cells, and mesenchymal cells in the AGM and the fetal liver by immunofluorescence assay (Fig. 4 B). The expression pattern of Pet1 suggested that 5-HT might be synthesized in the AGM de novo during embryogenesis.

Next, we examined the expression of the enzymes responsible for 5-HT synthesis. It is known that in the process of 5-HT synthesis, L-tryptophan is first converted into 5-HTP by Tph; then, 5-HTP is converted into 5-HT by AAAD. There are two isoforms of Tph in the mouse: Tph1 and Tph2 (Côté et al., 2003). Both *tph1* and *tph2* were expressed in the AGM (Fig. 4, C–F), but their expression levels were quite different. Compared with the levels in the whole embryo, *tph1* expression was much lower in the AGM (Fig. 4 G). In contrast, *tph2* was highly expressed (Fig. 4 H). A direct comparison of their expression in the AGM also showed that *tph2* expression was significantly increased compared with *tph1* (Fig. 4 I). These results show that *tph2* is highly expressed in the AGM, indicating that *tph2* but not *tph1* might contribute to 5-HT synthesis in this region.

In addition, Tph2 and AAAD were coexpressed in endothelial cells, subaortic mesenchymal cells, and a subset of hematopoietic cells (Fig. 4 J). Based on these results, we further analyzed the location of 5-HT in the AGM. 5-HT was located in the IAHC, endothelial cells, subaortic mesenchymal cells, and also in rare hematopoietic cells (Fig. 4 K). Together, these data suggest that 5-HT is biosynthesized in the AGM during embryogenesis.

The level of 5-HT in the brain has been reported to gradually decrease in *tph2*$^{+/-}$ and *tph2*$^{-/-}$ embryos (Liu et al., 2011). Liquid chromatography–mass spectrometry (LC-MS) quantitatively confirmed that the concentration of 5-HT in the AGM was decreased in *tph2*$^{+/-}$ embryos and was the lowest in *tph2*$^{-/-}$ embryos (Fig. 4 L). The 5-HT concentration in the AGM was decreased from ∼18 ng/g in *tph2*$^{+/+}$ embryos to ∼4.5 ng/g in *tph2*$^{-/-}$ embryos. This directly supports the main contribution of *tph2* to the production of 5-HT in the AGM. Consistently, 5-HT staining further showed that the level of 5-HT was decreased in the AGM of *tph2*$^{+/-}$ and *tph2*$^{-/-}$ embryos compared with the controls (Fig. 4 M). A sequential decrease in 5-HT was observed in the AGM of *pet1*-cre;*tph2*$^{+/fl}$ and *pet1*-cre;*tph2*$^{fl/fl}$ embryos (Fig. 4 N, top).

in the DA of *tph2*$^{+/fl}$ and *vec*-cre;*tph2*$^{+/fl}$ embryos. *n* = 3. (L) Quantification of hematopoietic clusters (yellow arrowhead shown in J) in the DA of *tph2*$^{+/fl}$ and *vec*-cre;*tph2*$^{+/fl}$ embryos. *n* = 3. (M) AGMs from *tph2*$^{+/+}$ and *tph2*$^{+/-}$ embryos at E11.5 were dissociated with collagenase and directly transplanted into irradiated adult recipients at 0.5 tissue per recipient. CFU-S_{11} colonies were scored in positive recipients. *n* = 4. (N) Graph showing the percentage of donor chimerism in bone marrow of adult recipients (CD45.1) >4 mo after transplantation. AGMs from *tph2*$^{+/+}$ or *tph2*$^{+/-}$ E11.5 embryos (CD45.2) were dissociated with collagenase and directly transplanted as 1 ee into irradiated adult recipients. *n* = 5. The results are presented as mean ± SE. Student's *t* test: *, P < 0.05; **, P < 0.01; ***, P < 0.001.

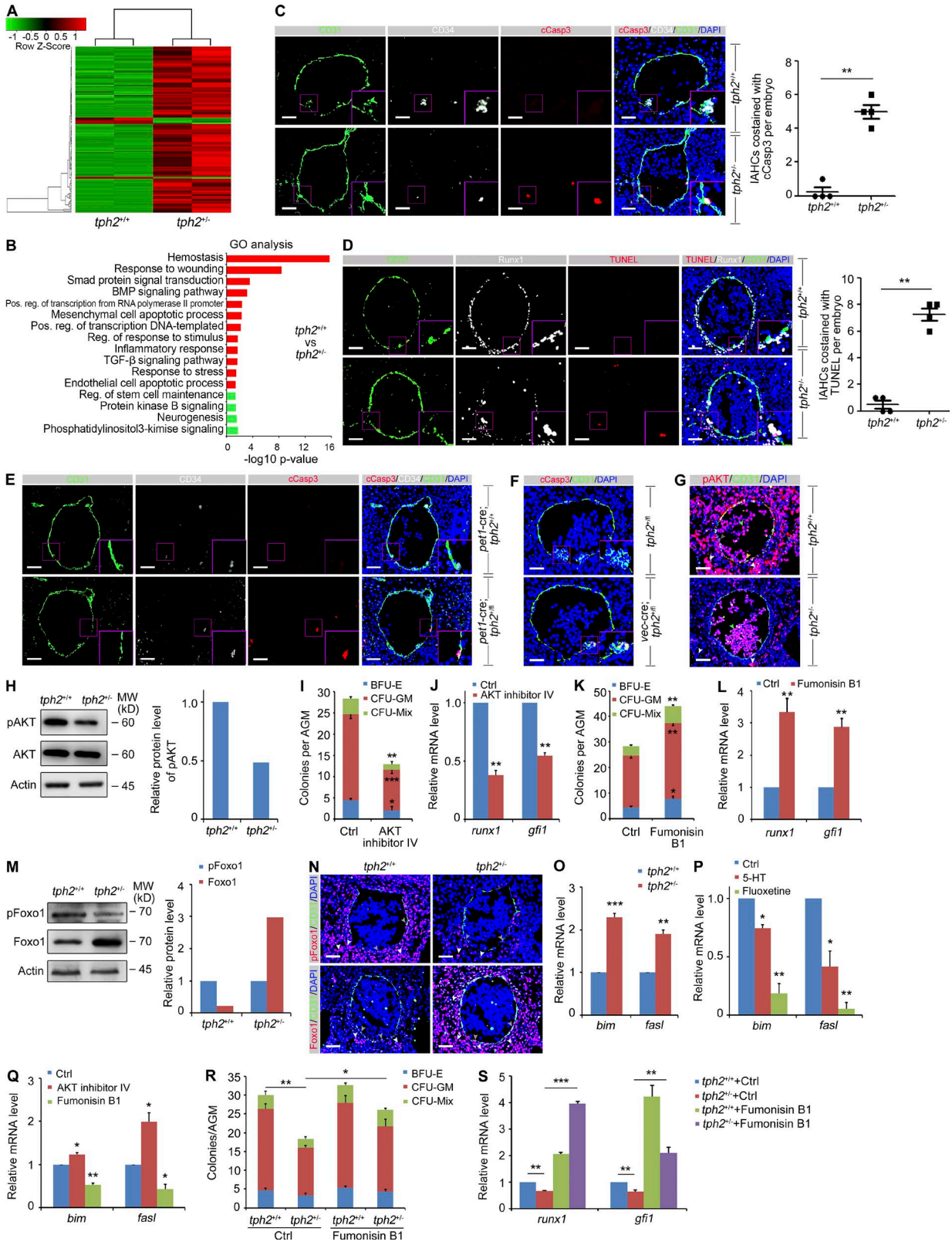

Figure 3. **Up-regulation of the apoptotic pathway suppresses the survival of HSPCs in hematopoietic clusters of *tph2*$^{+/-}$ embryos.** (A) The AGMs of *tph2*$^{+/+}$ and *tph2*$^{+/-}$ embryos at E11.5 were used for RNA-Seq analysis. The heat map shows the deregulated expressed genes enriched in GO analysis. (B) GO analysis showing the enrichment of up-regulated and down-regulated genes in RNA-Seq analysis. (C) Immunofluorescence assay with anti-cCasp3,

Importantly, the 5-HT level was also orderly decreased in *vec*-cre;*tph2*$^{+/fl}$ and *vec*-cre;*tph2*$^{fl/fl}$ embryos (Fig. 4 N, bottom). Together, these data suggest that the 5-HT synthesized in the endothelial cells of the AGM is important for HSPC survival.

Htr5a is responsible for 5-HT signaling during HSPC development

Through its receptors on the cell membrane, 5-HT activates the intracellular second messenger cascade, although the receptors that are highly enriched in the AGM and participate in regulating HSPC development have not yet been reported. As shown in Fig. 5 A, *htr2a* and *htr5a* were both highly expressed in the AGM compared with non-AGM tissues. We performed immunofluorescence assay on E10.5 and E11.5 embryo sections to determine the cell types expressing Htr2a and Htr5a. Htr5a was expressed in the IAHC, endothelial cells, subaortic mesenchymal cells, a small number of hematopoietic cells, and in the fetal liver (Fig. 5 B), which was quite similar to Pet1 expression (Fig. 4 B), whereas Htr2a was only expressed in hematopoietic cells (Fig. 5 C). Based on the expression patterns of Htr2a and Htr5a, we speculated that 5-HT mainly regulates the survival of HSPCs through Htr5a in mice.

SB699551, a selective antagonist of Htr5a, was used to test this hypothesis. Inhibition of Htr5a clearly decreased AKT and Foxo1 phosphorylation and consequently up-regulated Foxo1 expression (Fig. 5 D). The proapoptotic genes *bim* and *fasl* were up-regulated in the AGM, whereas *runx1* and *gfi1* were decreased upon Htr5a inhibition (Fig. 5, E and F); in addition, the colony numbers in the CFU-C assay were reduced by Htr5a inhibition (Fig. 5 G). These results suggest that Htr5a participates in 5-HT–dependent regulation of HSPC survival via the AKT-Foxo1 cascade.

Up-regulated Pet1-ERK signaling promotes HSPC proliferation and maintains normal HSPC development in *tph2*$^{-/-}$ embryos

We also examined the development of HSPCs in *tph2*$^{-/-}$ embryos in detail. As expected, the level of 5-HT in the AGM was further decreased compared with *tph2*$^{+/-}$ embryos (Fig. 4, L and M). Surprisingly, Runx1 staining showed no obvious change in the number of Runx1-positive cells and hematopoietic clusters in the *tph2*$^{-/-}$ AGM at E10.5 and E11.0, respectively (Fig. 6, A and B). The expression of *runx1* and *gfi1* in *tph2*$^{-/-}$ embryos was also unaffected (Fig. 6 C). A similar phenotype could also be observed in *pet1*-cre; *tph2*$^{fl/fl}$ embryos at E10.5 (Fig. 6, D–F). These results indicate that HSPC development is relatively normal in *tph2*$^{-/-}$ and *pet1*-cre;*tph2*$^{fl/fl}$ embryos.

Next, cell apoptosis was examined in the *tph2*$^{-/-}$ AGM, as it was the main cause of the impairments in definitive hematopoiesis in *tph2*$^{+/-}$ embryos. Anti-cCasp3 antibody staining showed that cell apoptosis of the CD31^{+}CD34^{+} cells in the IAHC was still evident in *tph2*$^{-/-}$ embryos compared with control embryos (Fig. 6, G and H). The expression of *bim* and *fasl* in *tph2*$^{-/-}$ embryos was also increased (Fig. 6 I). This result showed that the excessive apoptosis of HSPCs caused by the decrease in 5-HT levels remained present in *tph2*$^{-/-}$ embryos.

We examined *tph1* expression in *tph2*$^{-/-}$ embryos to determine whether *tph1* and *tph2* have redundant functions in the AGM. There was no change in *tph1* expression at the mRNA level in the AGM of *tph2*$^{-/-}$ embryos (Fig. 6 J). Consistently, there was no difference in the level of the Tph1 protein in the AGM, trunk, and head regions among the three genotypes of embryos (Fig. 6 K). This result agreed with a previous study showing no compensatory up-regulation of Tph1 in a *tph2* knockout mouse (Kriegebaum et al., 2010).

E11.5 AGMs of *tph2*$^{+/+}$, *tph2*$^{+/-}$, and *tph2*$^{-/-}$ embryos were obtained for RNA-Seq analysis to explore the under-

anti-CD31, and anti-CD34 antibodies on the sections of *tph2*$^{+/+}$ (top) and *tph2*$^{+/-}$ (bottom) embryos at E10.5. (Right) Quantification of IAHCs costained with cCasp3 per embryo. Bars, 10 µm. *n* = 4. (D) TUNEL assay on the sections of *tph2*$^{+/+}$ (top) and *tph2*$^{+/-}$ (bottom) embryos at E10.5. (Right) Quantification of IAHCs costained with TUNEL (terminal deoxynucleotidyl transferase deoxyuridine triphosphate nick-end labeling) per embryo. Bars, 10 µm. *n* = 4. (E) Immunofluorescence assay with anti-cCasp3, anti-CD31, and anti-CD34 antibodies on the sections of *pet1*-cre;*tph2*$^{+/+}$ (top) and *pet1*-cre;*tph2*$^{+/fl}$ (bottom) embryos at E10.5. Bars, 10 µm. (F) Immunofluorescence assay with anti-cCasp3 and anti-CD31 antibodies on the sections of *tph2*$^{+/fl}$ (top) and *vec*-cre;*tph2*$^{+/fl}$ (bottom) embryos at E10.5. The hematopoietic clusters in *vec*-cre;*tph2*$^{+/fl}$ embryos tended to be apoptotic. Bars, 10 µm. (G) Phosphorylation of AKT (pAKT) in the AGM of *tph2*$^{+/+}$ and *tph2*$^{+/-}$ embryos at E10.5 was detected by immunofluorescence assay. The results show the location of pAKT in the endothelial cells (gray arrowheads), hematopoietic clusters (yellow arrowhead), mesenchymal cells (white arrowheads), and hematopoietic cells (green arrowheads). Bars, 10 µm. (H) Western blot results further confirmed the expression of pAKT in the AGM of *tph2*$^{+/-}$ embryos at E10.5. (Right) Quantification of the Western blot results. *n* = 3. (I and J) The AGMs were treated with AKT inhibitor at 10 µm, and then, the number of colonies in the CFU-C assay was counted, and the expression of *runx1* and *gfi1* was detected by qPCR analysis. *n* = 3. (K and L) The AGMs were treated with AKT activator at 10 µM, and then the colony numbers in the CFU-C assay were counted, and the expression of *runx1* and *gfi1* was detected by qPCR analysis. *n* = 3. (M) Phosphorylation of Foxo1 and total Foxo1 were detected in the AGM of *tph2*$^{+/-}$ embryos by Western blot analysis. (Right) Quantification of the Western blot results. *n* = 3. (N) Immunofluorescence assay confirmed the expression of pFoxo1 and Foxo1 in the endothelial cells (gray arrowheads) and mesenchymal cells (white arrowheads) in the AGM of *tph2*$^{+/-}$ embryos. Bars, 10 µm. (O) qPCR analysis showed the mRNA levels of *bim* and *fasl* in the AGM of *tph2*$^{+/-}$ embryos at E10.5. *n* = 3. (P and Q) qPCR analysis was performed using the AGMs treated with different chemicals including 5-HT, fluoxetine, Fumonisin B1 (AKT activator), and inhibitor of AKT by AGM explant culture system. *n* = 3. (R) CFU-C assay using the AGMs of *tph2*$^{+/+}$ and *tph2*$^{+/-}$ embryos at E10.5 treated with Fumonisin B1 at 10 µM. 1 ee was used. *n* = 3. (S) qPCR was performed using the AGMs of *tph2*$^{+/+}$ and *tph2*$^{+/-}$ embryos at E10.5 treated with Fumonisin B1. *n* = 3. The results are presented as mean ± SE. Student's *t* test: *, P < 0.05; **, P < 0.01; ***, P < 0.001. BFU-E, burst forming unit-erythroid; CFU-GM, CFU-granulomonocyte; Ctrl, control; MW, molecular weight; Pos. positive; reg. regulation.

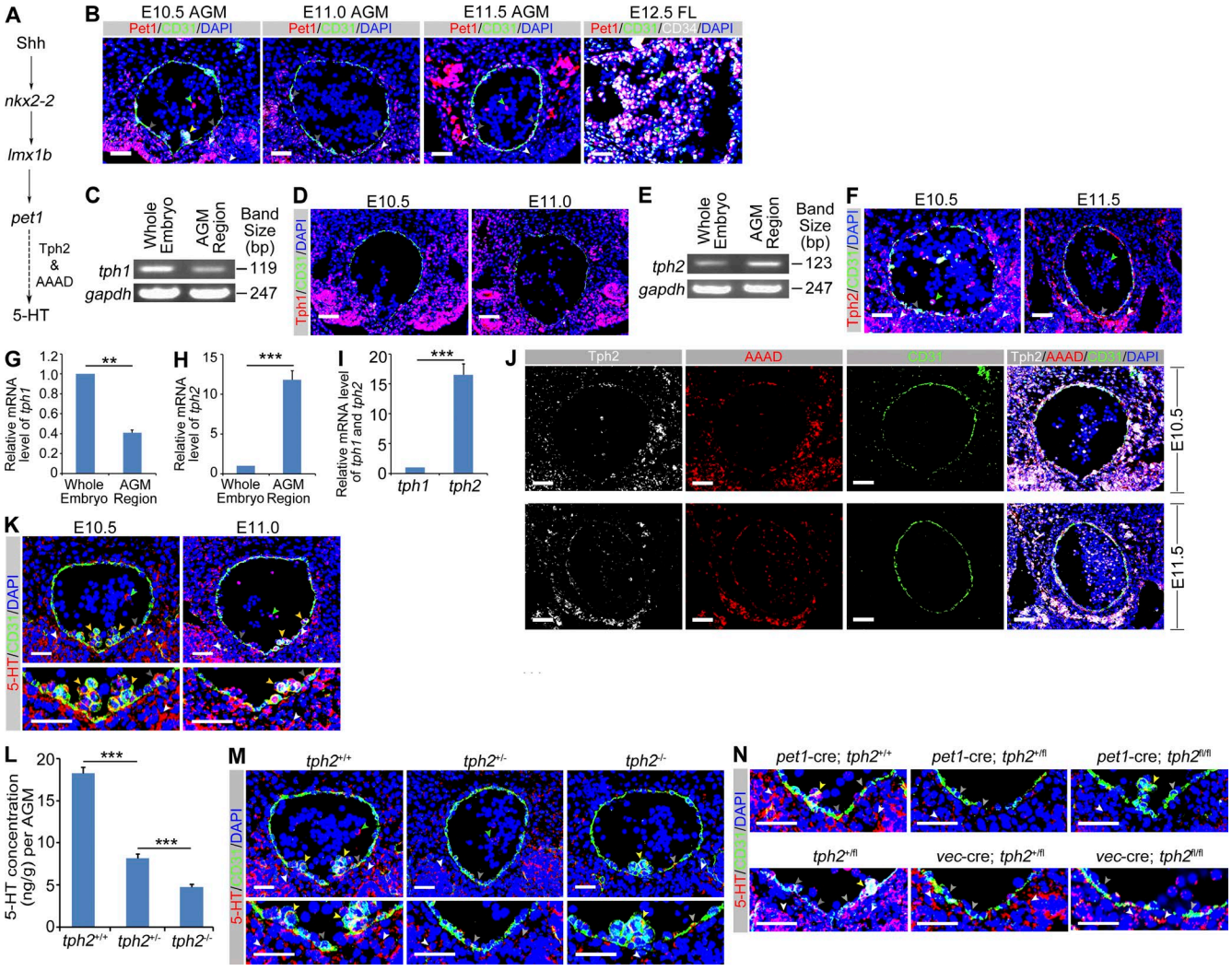

Figure 4. **5-HT is biosynthesized in the AGM and regulates definitive hematopoiesis in mouse embryos.** (A) Flow chart showing that 5-HT synthesis was controlled by Shh signaling and *nkx2-2–lmx1b-pet1* cascade. Tph, and AAAD were two important enzymes for 5-HT synthesis. (B) Immunofluorescence analysis on embryo sections showing the expression pattern of Pet1 in the AGM of mouse embryos at E10.5, E11.0, and E11.5 and in the fetal liver of embryos at E12.5. Endothelial cells were stained with anti-CD31 antibody. Bars, 10 µm. (C) Expression of *tph1* in the AGM of embryos was detected by RT-PCR. (D) Immunofluorescence analysis on embryo sections was used to detect the expression of Tph1 in the AGM of mouse embryos at E10.5 and E11.0. Endothelial cells were stained with anti-CD31 antibody. Bars, 10 µm. (E) Expression of *tph2* in the AGM of embryos was detected by RT-PCR. (F) Immunofluorescence analysis on embryo sections was used to detect the expression pattern of Tph2 in the AGM of mouse embryos at E10.5 and E11.5. Endothelial cells were stained with anti-CD31 antibody. Bars, 10 µm. (G) qPCR was performed to confirm the expression of *tph1* in the AGM. (H) qPCR analysis of *tph2* expression in the AGM. (I) qPCR analysis of *tph1* and *tph2* expression in the AGM. (J) Immunofluorescence analysis on embryo sections using anti-Tph2 and anti-AAAD antibodies to detect the colocation of Tph2 and AAAD in the AGM. Endothelial cells were stained with anti-CD31 antibody. Bars, 10 µm. (K) Immunofluorescence analysis on E10.5 and E11.0 wild-type embryo sections with antibody to 5-HT to detect the location of 5-HT in the AGM. Endothelial cells were stained with anti-CD31 antibody. Bars, 10 µm. (L) LC-MS was performed using the AGMs of $tph2^{+/+}$, $tph2^{+/-}$, and $tph2^{-/-}$ embryos at E10.5 to detect the concentration of 5-HT. (M) Immunofluorescence analysis on sections to detect the location of 5-HT in the AGM of $tph2^{+/+}$, $tph2^{+/-}$, and $tph2^{-/-}$ embryos at E10.5. Endothelial cells were stained with anti-CD31 antibody. Bars, 10 µm. (N) The level of 5-HT in hematopoietic clusters (yellow arrowheads), endothelial cells (gray arrowheads), and subaortic mesenchymal cells (white arrowheads) was detected in *pet1*-cre;$tph2^{+/fl}$ and *pet1*-cre;$tph2^{fl/fl}$ embryos (top) and in *vec*-cre;$tph2^{+/fl}$ and *vec*-cre;$tph2^{fl/fl}$ embryos (bottom). Endothelial cells were stained with anti-CD31 antibody. Bars, 10 µm. The results are presented as mean ± SE. Student's *t* test: **, $P < 0.01$; ***, $P < 0.001$. $n = 3$. Gray arrowheads indicate endothelial cells, yellow arrowheads indicate hematopoietic clusters, white arrowheads indicate mesenchymal cells, and green arrowheads indicate hematopoietic cells.

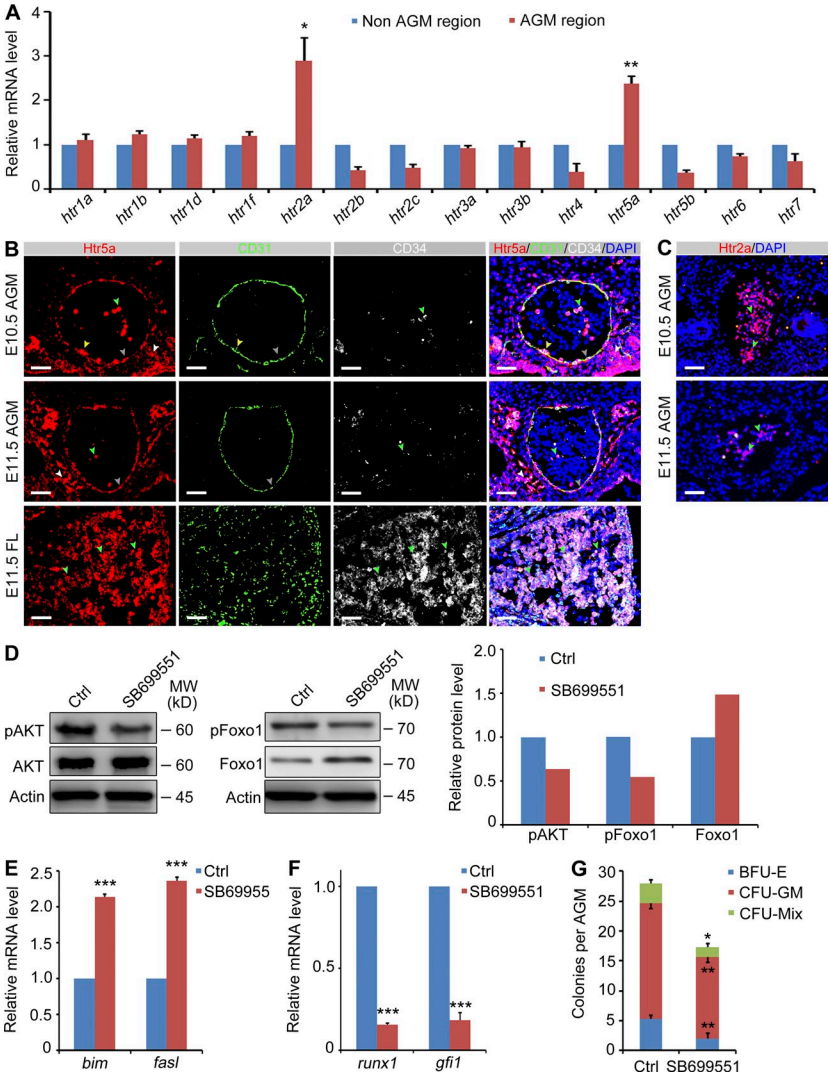

Figure 5. **Htr5a is responsible for 5-HT regulating the survival of HSPCs.** (A) qPCR analysis was performed to detect the expression of 5-HT receptors in the AGM. (B) Immunofluorescence on sections with anti-Htr5a, anti-CD31, and anti-CD34 antibodies in the AGM of embryos at E10.5 and E11.5. Bars, 10 µm. (C) Immunofluorescence on sections with anti-Htr2a antibody in the AGM of wild-type embryos at E10.5 and E11.5. Bars, 10 µm. (B and C) Gray arrowheads indicate endothelial cells, yellow arrowheads indicate hematopoietic clusters, white arrowheads indicate mesenchymal cells, and green arrowheads indicate hematopoietic cells. (D) The phosphorylation of AKT and Foxo1 in SB699551-treated AGMs by Western blotting. (Right) Quantification of the Western blot results. $n = 3$. (E) Expression of *bim* and *fasl* in the AGM treated with SB699551 at 200 nM. (F) qPCR analysis showing the expression of *runx1* and *gfi1* in the AGM treated with SB699551. (G) CFU-C assay of AGMs treated SB699551. The number of colonies was counted. 1 ee was used. The results are presented as mean ± SE. Student's *t* test: *, $P < 0.05$; **, $P < 0.01$; ***, $P < 0.001$. $n = 3$. BFU-E, burst forming unit–erythroid; CFU-GM, CFU-granulomonocyte; Ctrl, control; FL, fetal liver; MW, molecular weight.

lying mechanism accounting for this unexpected phenotype. Genes that were only up-regulated in *tph2*$^{-/-}$ embryos compared with *tph2*$^{+/+}$ embryos, but not up-regulated in *tph2*$^{+/-}$ embryos, and enriched in the GO analysis are shown in Fig. 7 A and Table S3. Among them, cell apoptosis genes were enriched, consistent with the excessive HSPC apoptosis observed in *tph2*$^{-/-}$ embryos (Fig. 6, G–I).

Strikingly, the up-regulated genes in *tph2*$^{-/-}$ embryos were enriched in the regulation of hormone levels, smoothened signaling, MAPK cascade, and cell proliferation (Fig. 7, B–D). It has been reported that Shh signaling and the Nkx2-2–Lmx1b cascade lie upstream of Pet1 to regulate 5-HT production (Fig. 4 A; Ding et al., 2003). Our previous studies also showed that Pet1 regulates HSPC development via ERK signaling (Wang et al., 2013), and the precise ERK signaling strength is important for the development of HSPCs in zebrafish and mouse embryos (Zhang et al., 2014). Importantly, *shh* and *nkx2-2* were up-regulated in *tph2*$^{-/-}$ embryos but not in *tph2*$^{+/-}$ embryos in our RNA-Seq data (Fig. 7 A and Table S3), and the identified genes were enriched for cell proliferation (Fig. 7 C). Functional themes were also identified by a network visualization of the gene sets that were only enriched in *tph2*$^{-/-}$ embryos (Fig. 7 D). Genes involved in regulating hormone levels and cell proliferation were listed. Therefore, we speculated that in *tph2*$^{-/-}$ embryos, the severe decrease in 5-HT levels might stimulate the upstream signals and genes responsible for 5-HT synthesis, i.e., Shh signaling might be reactivated to up-regulate the Pet1-ERK signaling cascade and accelerate cell proliferation. We examined *cycD1*, *cycD2*, and *cycE1* expression to test this hypothesis, and we found that the levels of these genes were increased in the AGM of *tph2*$^{-/-}$ and *pet1*-cre;*tph2*$^{fl/fl}$ embryos (Fig. 7 E). Cell proliferation and pERK expression in the IAHCs were increased in the AGM of *tph2*$^{-/-}$ and *pet1*-cre;*tph2*$^{fl/fl}$ embryos, as determined by staining with pH3 and pERK antibodies (Fig. 7 F). Moreover, the increased number of pH3-stained cells largely overlapped with the increased number of pERK-stained cells. Similar to the increased expression of *ptch1*,

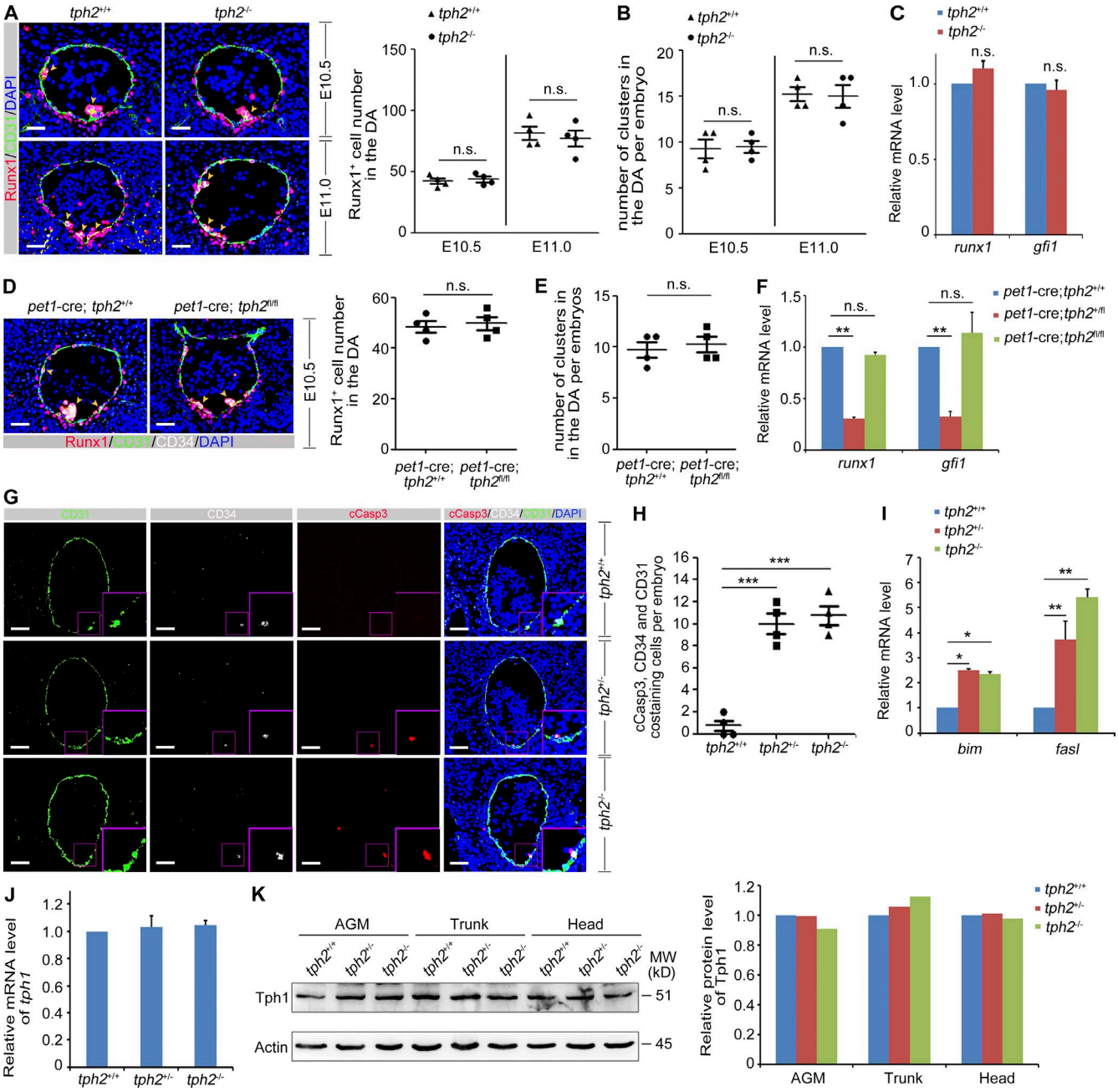

Figure 6. **Normal definitive hematopoiesis in *tph2*$^{-/-}$ embryos is not caused by the rescue of cell apoptosis and compensation of Tph1.** (A) Immunofluorescence analysis on sections of *tph2*$^{+/+}$ and *tph2*$^{-/-}$ embryos at E10.5 and E11.0 with anti-Runx1 and anti-CD31 antibodies. IAHC is marked with yellow arrowheads. Bars, 10 µm. (Right) Quantification of Runx1-positive cells in the DA of the sections. $n = 4$. (B) Quantification of hematopoietic clusters (yellow arrowhead shown in A) in the DA of *tph2*$^{+/+}$ and *tph2*$^{-/-}$ embryos at E10.5 and E11.0. $n = 4$. (C) qPCR analysis showed that the expression of *runx1* and *gfi1* in the AGM of *tph2*$^{+/+}$ and *tph2*$^{-/-}$ embryos at E10.5. $n = 3$. (D, left) Immunofluorescence analysis on sections of *pet1*-cre;*tph2*$^{+/+}$ and *pet1*-cre;*tph2*$^{fl/fl}$ embryos at E10.5 with anti-CD31, anti-CD34, and anti-Runx1 antibodies. IAHC is marked with yellow arrowheads. Bars, 10 µm. (Right) Quantification of Runx1-positive cells in the DA of the sections. $n = 4$. (E) Quantification of hematopoietic clusters (yellow arrowhead shown in D) in the DA of *pet1*-cre;*tph2*$^{+/+}$ and *pet1*-cre;*tph2*$^{fl/fl}$ embryos at E10.5. $n = 4$. (F) qPCR analysis showed the mRNA levels of *runx1* and *gfi1* in the AGM of *pet1*-cre;*tph2*$^{+/fl}$ and *pet1*-cre;*tph2*$^{fl/fl}$ embryos compared with the controls at E10.5. $n = 3$. (G) Immunofluorescence assay with anti-cCasp3, anti-CD31, and anti-CD34 antibodies on the sections of *tph2*$^{+/+}$ (top), *tph2*$^{+/-}$ (middle), and *tph2*$^{-/-}$ (bottom) embryos at E11.5. Bars, 10 µm. (H) Quantification of IAHCs costained with cCasp3 per embryo. $n = 4$. (I) Expression of *bim* and *fasl* in the AGM of *tph2*$^{+/+}$, *tph2*$^{+/-}$, and *tph2*$^{-/-}$ embryos at E10.5 detected by qPCR. $n = 3$. (J) qPCR analysis showed the expression of *tph1* in the AGM of *tph2*$^{+/-}$ and *tph2*$^{-/-}$ embryos at E10.5. (K) Western blot analysis was performed to detect the expression of Tph1 in the AGM, trunk, and head region of *tph2*$^{+/+}$, *tph2*$^{+/-}$, and *tph2*$^{-/-}$ embryos at E10.5. (Right) Quantification of the Western blot results. n = at least 2. The results are presented as mean ± SE. Student's *t* test: *, $P < 0.05$; **, $P < 0.01$; ***, $P < 0.001$.

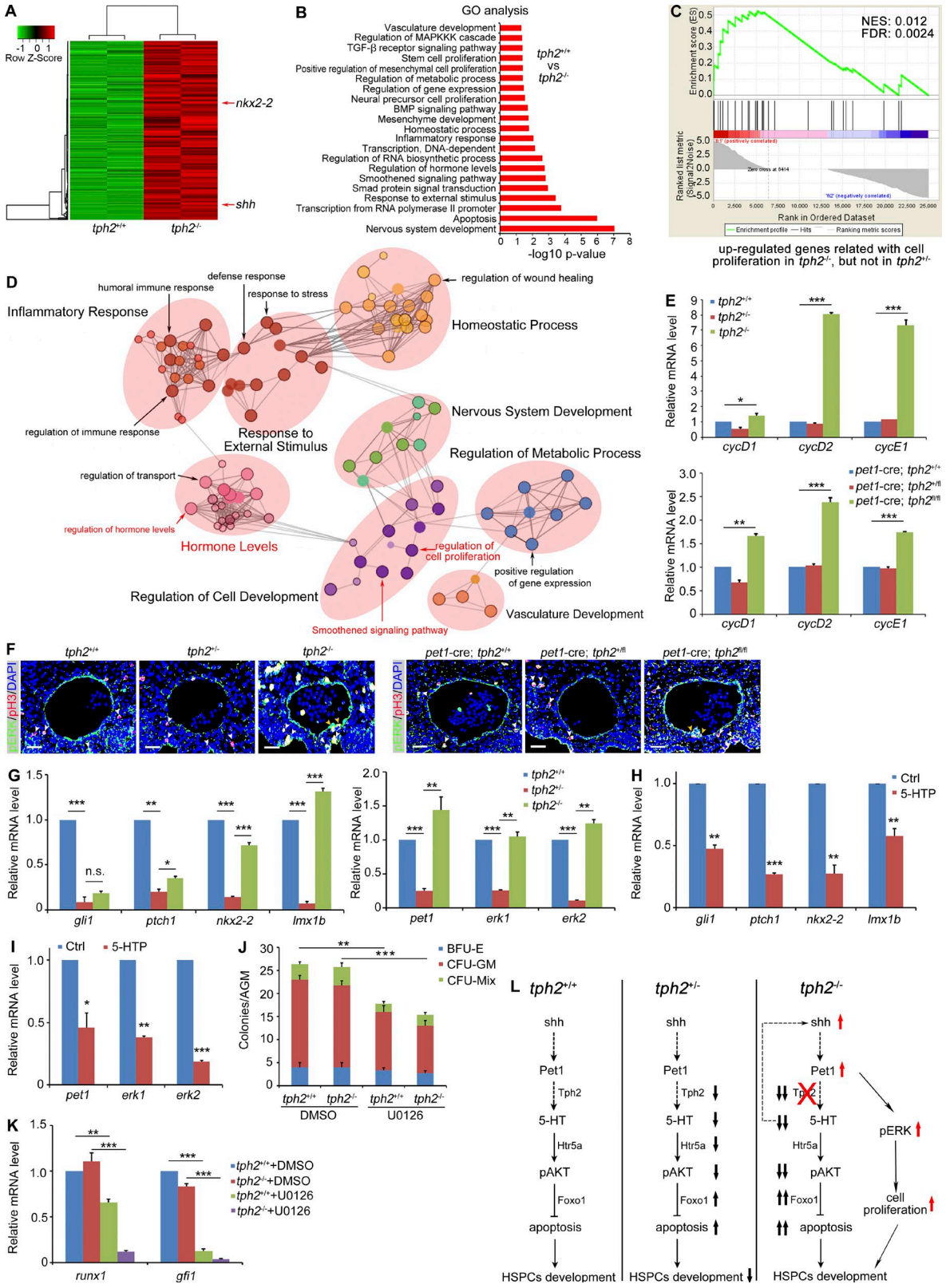

Figure 7. **Increase of cell proliferation in hematopoietic clusters maintains relatively normal definitive hematopoiesis in *tph2*$^{-/-}$ embryos.** (A) The AGMs of *tph2*$^{+/+}$, *tph2*$^{+/-}$, and *tph2*$^{-/-}$ embryos at E11.5 were subjected to RNA-Seq analysis. The up-regulated genes enriched in GO analysis are shown in the heat map. All of these genes were sequenced to be only up-regulated in *tph2*$^{-/-}$ embryos but not in *tph2*$^{+/-}$ embryos. (B) GO analysis showing the

nkx2-2, and *lmx1b*, the mRNA levels of *pet1* and *erk* were also up-regulated in *tph2*$^{-/-}$ embryos compared with *tph2*$^{+/-}$ embryos (Fig. 7 G). Our in vitro experiment further showed that 5-HTP (the precursor of 5-HT) treatment down-regulated the transcription of *gli1*, *ptch1*, *nkx2-2*, *lmx1b*, *pet1*, and *erk* (Fig. 7, H and I). The CFU-C assay with E10.5 *tph2*$^{+/+}$ and *tph2*$^{-/-}$ AGMs further showed that inhibition of ERK signaling with U0126 (MEK1/2 inhibitor) decreased the colony number and the expression of *runx1* and *gfi1* in *tph2*$^{-/-}$ embryos (Fig. 7, J and K).

Collectively, these results showed that the Nkx2-2–Lmx1b-Pet1 cascade and the upstream Shh signaling pathway were up-regulated in *tph2*$^{-/-}$ embryos, which in turn reactivated Pet1-ERK signaling. This activated ERK signaling in *tph2*$^{-/-}$ embryos promoted the proliferation of hematopoietic clusters and, thereby, partially restored the defective HSPC development observed in *tph2*$^{+/-}$ embryos (Fig. 7 L).

DISCUSSION

5-HT is perhaps most well known as a neurotransmitter that affects a variety of central functions, but it also plays important roles outside the CNS (Berger et al., 2009). Since it was discovered 60 yr ago (Rapport et al., 1948), increasing evidence has reported the expression and function of 5-HT and its receptors in peripheral tissues. The roles of 5-HT in early embryonic development, including craniofacial morphogenesis and patterning of the left–right axis, have been reported (Fukumoto et al., 2005; Reisoli et al., 2010). In this work, for the first time, we have shown that the low-grade decrease in 5-HT levels in *tph2* haploinsufficient embryos leads to a remarkable impairment of HSPC development. 5-HT is biosynthesized in the AGM and is important for the survival of HSPC in the IAHC. Mechanistically, we identified that AKT-Foxo1 signaling controls the survival of HSPCs downstream of Htr5a, the 5-HT receptor (Fig. 7 L).

Previously, we showed that Fev (Pet1 in mammals) regulates HSPC development in zebrafish via ERK signaling (Wang et al., 2013). The well-known role of Pet1 is to control 5-HT synthesis (Hendricks et al., 2003). Interestingly, Pet1, Tph2, and AAAD, the transcription factor and enzymes responsible for 5-HT synthesis, are all expressed in the AGM, and 5-HT synthesis is readily observed in situ. Together, these results imply that 5-HT may cell autonomously contribute to HSPC development. Our experiments in *tph2*$^{+/-}$, *pet1*-cre;*tph2*$^{+/fl}$, and *vec*-cre;*tph2*$^{+/fl}$ embryos revealed that 5-HT actually regulates the survival of emerging HSPCs in the AGM. In addition to 5-HT, other neurotransmitters or hormones have been reported to be involved in HSPC development and/or maintenance. The sympathetic nervous system is the well-studied neural system that regulates embryonic or adult hematopoiesis. A previous study has shown that catecholamine, which is derived from the sympathetic nervous system in the AGM, regulates HSPC development in mouse embryos (Fitch et al., 2012). Studies in bone marrow also showed that catecholamine regulates HSPC proliferation and migration (Katayama et al., 2006; Méndez-Ferrer et al., 2008). Prostaglandin E2 has been reported to be required for HSC formation in zebrafish embryos and can increase the reconstitution ability of HSCs in mouse bone marrow (North et al., 2007). Prostaglandin E2 was further identified as an important hormone that regulates HSC development during embryogenesis and organ regeneration by modifying Wnt signaling (Goessling et al., 2009). Therefore, our findings in this work provide additional data to support the role of neurotransmitters or hormones in HSPC development and function.

A recent publication reported that 5-HT plays an essential role in HSPC development in zebrafish embryos (Kwan et al., 2016). It showed that CNS-derived 5-HT increased the number of embryonic HSPCs through the hypothalamic-pituitary-adrenal/interregnal axis. However, we demonstrated in this work that 5-HT is synthesized in the endothelial cells of the AGM in mice and regulates HSPC production through its receptor Htr5a expressed on HSPCs, suggesting a direct and local effect of 5-HT signaling in HSPC development. Our previous study showed that *tph2* is expressed in endothelial cells, HE cells, and HSPCs in the AGM region of zebrafish (Zhang et al., 2015). Consistent with the results in zebrafish, we verified that *tph2* was also highly expressed and contrib-

enrichment of genes only up-regulated in *tph2*$^{-/-}$ embryos by RNA-Seq. (C) Gene set enrichment analysis for genes only up-regulated in *tph2*$^{-/-}$ embryos related with cell proliferation. (D) Functional themes were identified by network visualization of gene sets only enriched in *tph2*$^{-/-}$ embryos. (E) Expression of *cycD1*, *cycD2*, and *cycE1* in the AGM of *tph2*$^{+/+}$, *tph2*$^{+/-}$, and *tph2*$^{-/-}$ embryos (top) and *pet1*-cre;*tph2*$^{+/+}$, *pet1*-cre;*tph2*$^{+/fl}$, and *pet1*-cre;*tph2*$^{fl/fl}$ embryos (bottom) at E10.5 were detected by qPCR. (F) Immunofluorescence analysis on sections to detect the costaining of pERK and pH3 in the AGMs of *tph2*$^{+/+}$, *tph2*$^{+/-}$, and *tph2*$^{-/-}$ embryos (left) and *pet1*-cre;*tph2*$^{+/+}$, *pet1*-cre;*tph2*$^{+/fl}$, and *pet1*-cre;*tph2*$^{fl/fl}$ embryos (right) at E10.5. Costaining of pERK and pH3 in IAHCs and mesenchymal cells are marked with yellow arrowheads and white arrowheads, respectively. Bars, 10 µm. (G) qPCR analysis showed the expression of *gli1*, *ptch1*, *nkx2-2*, *lmx1b*, *pet1*, *erk1*, and *erk2* in the AGM of *tph2*$^{+/+}$, *tph2*$^{+/-}$, and *tph2*$^{-/-}$ embryos at E10.5. (H) Expression of *gli1*, *ptch1*, *nkx2-2*, and *lmx1b* in the AGMs treated with 5-HTP. (I) Expression of *pet1*, *erk1*, and *erk2* in the AGMs treated with 5-HTP. (J) CFU-C assay using the AGMs of *tph2*$^{+/+}$ and *tph2*$^{-/-}$ embryos at E10.5 treated with U0126 (MEK1/2 inhibitor) at 1 µM. 1 ee was used. (K) qPCR analysis of expression of *runx1* and *gfi1* in E10.5 AGMs of *tph2*$^{+/+}$ and *tph2*$^{-/-}$ embryos treated with U0126 at 1 µM. (L) Model to explain the different hematopoietic phenotypes in *tph2*$^{+/-}$ and *tph2*$^{-/-}$ embryos. The proapoptotic pathway was up-regulated through the Htr5a-AKT-Foxo1 axis, which led to the impaired survival of HSPCs in *tph2*$^{+/-}$ embryos. However, in *tph2*$^{-/-}$ embryos, genes involved in regulating synthesis of 5-HT were up-regulated. We propose that the reactivated Pet1-ERK signaling cascade in *tph2*$^{-/-}$ embryos thereby promoted the proliferation of HSPCs in hematopoietic clusters and partially restored the defective HSPC development observed in *tph2*$^{+/-}$ embryos. The results are presented as mean ± SE. Student's *t* test: *, $P < 0.05$; **, $P < 0.01$; ***, $P < 0.001$. $n = 3$. Ctrl, control; FDR, false discovery rate; NES, net enrichment score.

uted to the main synthesis of 5-HT in the AGM of mice. The 5-HT levels in these cells were decreased in *tph2* haploinsufficient embryos. The expression of *tph2* in the AGM clearly revealed that *tph2* is expressed not only in the CNS, but also in the peripheral tissues. This result is opposite to that of *tph1*, which is highly expressed in the peripheral tissues, such as the skin, gut, and pineal gland, but is also expressed at low levels in the CNS (Zill et al., 2009). More importantly, the mRNA level of *tph2* is much higher than that of *tph1*, and most of 5-HT disappeared in the $tph2^{-/-}$ AGM. Therefore, *tph2* but not *tph1* mainly contributes to 5-HT synthesis in the AGM.

Surprisingly, the development of HSPCs in $tph2^{-/-}$ embryos was relatively normal. Genes that were only up-regulated in $tph2^{-/-}$ embryos were enriched in the regulation of neurotransmitter or hormone levels and cell proliferation. RNA-Seq and biochemical analyses indicated that the severe decrease in the 5-HT levels in $tph2^{-/-}$ embryos up-regulated the expression of Pet1, possibly through the Shh–Nkx2-2–Lmx1b cascade feedback mechanism. The Shh–Nkx2-2–Lmx1b-Pet1 cascade has been identified as a classical pathway that regulates 5-HT synthesis in the CNS (Ding et al., 2003). Interestingly, we observed *pet1* up-regulation and increased activation of ERK signaling in the $tph2^{-/-}$ AGM, which was directly regulated by *pet1* (Wang et al., 2013). Consequently, increased Pet1-ERK signaling in $tph2^{-/-}$ embryos promoted cell proliferation in the AGM, therefore compensating for the decreased number of HSPCs caused by excessive apoptosis due to the low levels of 5-HT. Further studies will be required to determine how the attenuated 5-HT levels trigger up-regulation of Shh signaling in $tph2^{-/-}$ embryos.

It has been reported that the neurotrophic factor receptor RET promotes HSPC function by providing *bcl2* and *bcl2l1* survival signals in the adult hematopoietic system (Fonseca-Pereira et al., 2014). A recent study also showed that during embryogenesis, endothelial-specific deletion of chromodomain helicase DNA-binding protein 1 (Chd1) leads to the apoptosis of hematopoietic clusters at E10.5 and also hampers the maturation of c-$Kit^{+}CD45^{+}$ cells in vitro and in vivo (Koh et al., 2015). Consistently, our results strongly support the hypothesis that inhibition of the AKT-Foxo1–mediated proapoptotic pathway is important for protecting HSPCs in the AGM from apoptosis. Htr5a, the 5-HT receptor, is located on the cell membrane to transmit survival signals to nascent HSPCs. Many 5-HT receptors are the therapeutic targets of a variety of pharmaceutical drugs (Nichols and Nichols, 2008), and our results indicate that Htr5a might act as a potential target for the in vitro expansion of functional HSPCs.

MATERIALS AND METHODS

Animals

Wild-type C57BL/6 mice were purchased from Beijing HFK Bioscience Co. Ltd. *tph2* knockout mice (gift from Y. Rao, Peking University, Beijing, China), *vec*-cre mice (gift from B. Liu, Academy of Military Medical Sciences, Beijing, China), and *pet1*-cre;$tph2^{fl/fl}$ mice were as previously described (Gutknecht et al., 2008; Chen et al., 2009; Kriegebaum et al., 2010). The mice used in this study were housed under specific pathogen–free conditions and handled in accordance with institutional guidelines. Littermates were used as controls in experiments. The mice were used for timed matings, with the day on which the vaginal plug was detected considered as day 0. This study was approved by the Ethical Review Committee in the Institute of Zoology, Chinese Academy of Sciences.

Western blotting

The AGM regions from mouse embryos were homogenized with cell lysis buffer (10 mM Tris-HCl, pH 8.0, 10 mM NaCl, and 0.5% NP-40) containing protease inhibitor (no. 04693116001; Roche). Western blotting was performed as described previously (Wang et al., 2011). The protein levels of Runx1, Tph1, AKT, pAKT, Foxo1, and pFoxo1 were detected using the following antibodies: anti–β-actin antibody (1:2,000; Cell Signaling Technology), anti-Runx1 antibody (1:200; Abcam), anti-AKT antibody (1:1,000; Cell Signaling Technology), anti-pAKT antibody (1:2,000; Cell Signaling Technology), anti-Tph1 antibody (1:500; Abcam), anti-Foxo1 antibody (1:500; Abcam), and anti-pFoxo1 antibody (1:500; Abcam).

Immunofluorescence

Immunofluorescence assay for mouse embryos was performed as previously described (Zhang et al., 2014). $tph2^{+/+}$, $tph2^{+/-}$, or $tph2^{-/-}$ embryos, *pet1*-cre;$tph2^{+/+}$, *pet1*-cre;$tph2^{+/fl}$, and *pet1*-cre;$tph2^{fl/fl}$ embryos, and *vec*-cre;$tph2^{+/+}$, *vec*-cre;$tph2^{+/fl}$, and *vec*-cre;$tph2^{fl/fl}$ embryos at E10.5 and E11.0 were fixed with 4% paraformaldehyde in PBS for 6–8 h at 4°C. The slides were blocked with 5% BSA (0.3% Triton X-100) for 1 h at room temperature and incubated with anti-Runx1 antibody (1:500; Abcam), anti-CD31 antibody (1:600; Abcam), anti-CD34 antibody (1:100; Abcam), anti-Tph1 antibody (1:100; Abcam), anti-Tph2 antibody (1:100; Abcam), anti-AAAD antibody (1:50; Santa Cruz Biotechnology, Inc.), anti–5-HT antibody (1:2,000; Immunostar), anti-Htr2a antibody (1:50; Santa Cruz Biotechnology, Inc.), anti-Htr5a antibody (1:50; Santa Cruz Biotechnology, Inc.), anti-pAKT antibody (1:2,000; Cell Signaling Technology), anti-pH3 antibody (1:300; Cell Signaling Technology), anti-cCasp3 antibody (1:400; Cell Signaling Technology), anti-Pet1 antibody (1:100), anti-pERK antibody (1:200; Santa Cruz Biotechnology, Inc.), anti-Foxo1 antibody (1:500; Abcam), and anti-pFoxo1 antibody (1:500; Abcam) diluted in 1% BSA overnight at 4°C. After washing three times in PBS–Tween 20, the slides were incubated with anti–rabbit Ig fluorescein, anti–mouse Ig fluorescein, anti–goat Ig fluorescein, and anti–rat Ig fluorescein for 1 h at room temperature. The sections were counterstained with DAPI, and images were acquired by a confocal laser microscope (A1; Nikon).

Confocal microscopy

Confocal images were captured on a confocal laser microscope (A1; Nikon), and three-dimensional projections were generated using Nikon confocal software.

qPCR

Total RNAs were extracted from the AGM region of mouse embryos with TRNzol reagent (Tiangen) and were then reverse transcribed using M-MLV reverse transcription (Promega) to obtain cDNAs for use as qPCR templates. The qPCR assays were performed with a Bio-Rad system (CFX96), and the expression levels of *gapdh* for mouse embryos were used as the internal controls. The sequences of the primers used for qPCR and the lengths of the PCR products are listed in Table S1.

Flow cytometry analysis

E10.5 and E11.5 AGMs (35–40 sp and 45–47 sp, respectively) were dissociated with collagenase. Flow cytometry analysis was performed using MoFlo XDP (Beckman Coulter), as previously described (Lu et al., 2013).

LC-MS analysis

The LC-MS analysis of 5-HT was performed on a QTRAP 4500 LC-MS system (AB SCIEX). In brief, AGM regions of *tph2*$^{+/+}$, *tph2*$^{+/-}$, and *tph2*$^{-/-}$ embryos at E10.5 were obtained and used for the analysis as previously described (Carrera et al., 2007; Cannazza et al., 2012). The standard substance of 5-HT was purchased from Sigma-Aldrich. 5-HT was separated on a 4-µm liquid chromatography column (150 × 2 mm; Synergi; Hydro-RP 80 Å C18; Phenomenex) at 25°C column temperature. The elution solvent system was composed of 0.05% formic acid (solvent A) and acetonitrile (solvent B). The temperature of the autosampler was set at 4°C, and the injection volume was 5 µl. The gradient elution program was applied at a flow rate of 0.4 ml/min as follows: initial conditions of 95% (vol/vol) A held for 5 min, increased linearly to 0% (vol/vol) A in 10 min, held at 0% (vol/vol) A for 5 min, returned to initial conditions in 1 min, and maintained for 9 min.

Mass spectrometry was performed using electrospray ionization. Mass spectrometry analyses were conducted in positive-ion mode. The operating parameters were optimized as follows: collision gas (CUR), 15.0; collision gas (CAD), medium; IonSpray voltage (IS), 5,000 V; temperature, 550°C; ion source gas 1 (GS1), 50.0; ion source gas 2 (GS2), 50.0; declustering potential (DP), 50.0; entrance potential (EP), 8.0; collision energy (CE), 9.0; and collision cell exit potential (CXE), 13.0. Ion detection was performed in multiple reaction monitoring (MRM) mode where in m/z 177.0→159.9 [M-H]_ transition for 5-HT.

AGM explant cultures

AGM explant culture was performed as previously described (Fitch et al., 2012). E10 or E10.5 AGMs were dissected from the WT, *tph2*$^{+/+}$, *tph2*$^{+/-}$, or *tph2*$^{-/-}$ embryos and cultured on Durapore filters (EMD Millipore) at the air–liquid interface in M5300 long-term culture medium (STEMCELL Technologies). Different concentrations of chemicals were added to the medium. After 36–48-h culture, AGMs were used to quantify the mRNA level of hematopoietic related genes or protein level of Runx1. The remaining AGMs were dissociated with collagenase and used for CFU-C or CFU-S assays.

CFU-S assays

AGM cell preparations from *tph2*$^{+/+}$ and *tph2*$^{+/-}$ embryos at E11.5 were injected at 0.5 embryo equivalent (ee), and fluoxetine-treated AGM cell preparations were injected at 1 ee into irradiated (9 Gy) recipients. 11 d after transplantation, the spleens of the recipients were fixed with Bouin's solution, and the number of macroscopic colonies per spleen was determined.

mRNA sequencing analysis

Whole-genome gene expression analysis was performed using the AGMs from two littermate pairs of *tph2*$^{+/+}$, *tph2*$^{+/-}$, or *tph2*$^{-/-}$ embryos at E11.5. The total RNA was extracted using TRNzol (Tiangen), and cDNA samples were sequenced using a sequencing system (HiSeq3000; Illumina; RiboBio Co. Ltd). The reference *Mus musculus* genome and gene information were downloaded from the National Center for Biotechnology Information database. Sequencing-received raw image data were transformed by Base Calling into raw reads. Raw sequences were transformed into clean tags by solexaQA (Cox et al., 2010) by removing reads with low quality reads (such as >35% N in a read, redundancy, duplication, and ploy-A/T tails). Then, the saturation analysis was performed to check whether the number of detected genes increased along with sequencing amount (total tag number). The distribution of clean tag expressions was used to evaluate the normality of the whole data. After that, the remaining reads were aligned to the reference genome using software program TopHat 2.0.9 (Ghosh and Chan, 2016; Johns Hopkins University) with the following procedure: tophat –p 4 -library-type = fr-unstranded -G gtf. Then, we estimated gene expression based on RPKM (reads per kilobase transcript per million; Mortazavi et al., 2008) values for each sample by Cufflink (Ghosh and Chan, 2016). The cutoff value for determining gene transcriptional activity was determined based on a 95% confidence interval for all RPKM values for each gene. We defined these genes as DEGs. We applied the R package DEGseq to identify DEGs with the random sampling model based on the read count for each gene at different samples (Wang et al., 2010). P-value corresponds to differential gene expression test. The threshold of value in multiple tests was determined through manipulating the false discovery rate value. We used false discovery rate ≤0.05 as the threshold to judge the significance of DEGs. Based on DEGs, we used the BLAST2GO program to determine GO term. Pathway analysis was performed using the Kyoto Encyclopedia of Genes and Genomes annotation service KAAS (Moriya et al., 2007).

Long-term transplantation

AGM cell preparations from *tph2*$^{+/+}$ or *tph2*$^{+/-}$ (CD45.2) mice were intravenously injected into 8–10-wk-old male C57BL/6 (CD45.1) mice that had received a split dose of 9

Gy of x-ray irradiation. 4 mo later, the bone marrow was collected from the recipients. The mice were considered to exhibit successful reconstitution if the recipients demonstrated ≥10% donor-derived chimerism.

Statistical analysis

All experiments were performed at least three times. The data are reported as the means ± SEM. Student's *t* test was used for the statistical comparisons.

Accession no.

All sequencing data have been deposited in the National Center for Biotechnology Information's Gene Expression Omnibus database under accession no. GSE90130.

Online supplemental material

Table S1 provides the primers used for qPCR analysis in this study. Tables S2 and S3 are available as Excel files. Table S2 contains a gene list including several DEGs enriched in the GO analysis in the AGM of *tph2*$^{+/+}$ and *tph2*$^{+/-}$ embryos. Table S3 contains the genes that are only up-regulated in *tph2*$^{-/-}$ embryos compared with *tph2*$^{+/+}$ embryos but not up-regulated in *tph2*$^{+/-}$ embryos and enriched in the GO analysis.

ACKNOWLEDGMENTS

We thank Minmin Luo and Wei Li for helpful discussions and critical reading of the paper. We thank Yi Rao and Bing Liu for providing reagents used in this work and Jiayue Xu for bioinformatics analysis.

This work was supported by the National Natural Science Foundation of China (grants 31271570, 31425016, and 81530004), the Ministry of Science and Technology of China (grant 2016YFA0100500), and the Strategic Priority Research Program of the Chinese Academy of Sciences (XDA01010110).

The authors declare no competing financial interests.

Author contributions: J. Lv and L. Wang performed mouse experiments. Y. Gao performed Western blot analysis. Y.-Q. Ding provided critical reagents. J. Lv, L. Wang, and F. Liu conceived the project, analyzed the data, and wrote the paper. All authors read and approved the final manuscript.

Submitted: 1 June 2015
Revised: 20 September 2016
Accepted: 14 December 2016

REFERENCES

Amireault, P., S. Hatia, E. Bayard, F. Bernex, C. Collet, J. Callebert, J.M. Launay, O. Hermine, E. Schneider, J. Mallet, et al. 2011. Ineffective erythropoiesis with reduced red blood cell survival in serotonin-deficient mice. *Proc. Natl. Acad. Sci. USA.* 108:13141–13146. http://dx.doi.org/10.1073/pnas.1103964108

Ben Arous, J., S. Laffont, and D. Chatenay. 2009. Molecular and sensory basis of a food related two-state behavior in *C. elegans*. *PLoS One.* 4:e7584. http://dx.doi.org/10.1371/journal.pone.0007584

Berger, M., J.A. Gray, and B.L. Roth. 2009. The expanded biology of serotonin. *Annu. Rev. Med.* 60:355–366. http://dx.doi.org/10.1146/annurev.med.60.042307.110802

Bertrand, J.Y., N.C. Chi, B. Santoso, S. Teng, D.Y. Stainier, and D. Traver. 2010. Haematopoietic stem cells derive directly from aortic endothelium during development. *Nature.* 464:108–111. http://dx.doi.org/10.1038/nature08738

Bianchi, M., C. Moser, C. Lazzarini, E. Vecchiato, and F. Crespi. 2002. Forced swimming test and fluoxetine treatment: in vivo evidence that peripheral 5-HT in rat platelet-rich plasma mirrors cerebral extracellular 5-HT levels, whilst 5-HT in isolated platelets mirrors neuronal 5-HT changes. *Exp. Brain Res.* 143:191–197. http://dx.doi.org/10.1007/s00221-001-0979-3

Boisset, J.C., and C. Robin. 2010. Imaging the founder of adult hematopoiesis in the mouse embryo aorta. *Cell Cycle.* 9:2489–2490. http://dx.doi.org/10.4161/cc.9.13.12319

Boitano, A.E., J. Wang, R. Romeo, L.C. Bouchez, A.E. Parker, S.E. Sutton, J.R. Walker, C.A. Flaveny, G.H. Perdew, M.S. Denison, et al. 2010. Aryl hydrocarbon receptor antagonists promote the expansion of human hematopoietic stem cells. *Science.* 329:1345–1348. http://dx.doi.org/10.1126/science.1191536

Cannazza, G., M.M. Carrozzo, A.S. Cazzato, I.M. Bretis, L. Troisi, C. Parenti, D. Braghiroli, S. Guiducci, and M. Zoli. 2012. Simultaneous measurement of adenosine, dopamine, acetylcholine and 5-hydroxytryptamine in cerebral mice microdialysis samples by LC-ESI-MS/MS. *J. Pharm. Biomed. Anal.* 71:183–186. http://dx.doi.org/10.1016/j.jpba.2012.08.004

Carrera, V., E. Sabater, E. Vilanova, and M.A. Sogorb. 2007. A simple and rapid HPLC-MS method for the simultaneous determination of epinephrine, norepinephrine, dopamine and 5-hydroxytryptamine: application to the secretion of bovine chromaffin cell cultures. *J. Chromatogr. B Analyt. Technol. Biomed. Life Sci.* 847:88–94. http://dx.doi.org/10.1016/j.jchromb.2006.09.032

Chen, M.J., T. Yokomizo, B.M. Zeigler, E. Dzierzak, and N.A. Speck. 2009. Runx1 is required for the endothelial to haematopoietic cell transition but not thereafter. *Nature.* 457:887–891. http://dx.doi.org/10.1038/nature07619

Christie, A.E., T.M. Fontanilla, V. Roncalli, M.C. Cieslak, and P.H. Lenz. 2014. Identification and developmental expression of the enzymes responsible for dopamine, histamine, octopamine and serotonin biosynthesis in the copepod crustacean *Calanus finmarchicus*. *Gen. Comp. Endocrinol.* 195:28–39. http://dx.doi.org/10.1016/j.ygcen.2013.10.003

Côté, F., E. Thévenot, C. Fligny, Y. Fromes, M. Darmon, M.A. Ripoche, E. Bayard, N. Hanoun, F. Saurini, P. Lechat, et al. 2003. Disruption of the nonneuronal tph1 gene demonstrates the importance of peripheral serotonin in cardiac function. *Proc. Natl. Acad. Sci. USA.* 100:13525–13530. http://dx.doi.org/10.1073/pnas.2233056100

Cox, M.P., D.A. Peterson, and P.J. Biggs. 2010. SolexaQA: At-a-glance quality assessment of Illumina second-generation sequencing data. *BMC Bioinformatics.* 11:485. http://dx.doi.org/10.1186/1471-2105-11-485

Delaney, C., S. Heimfeld, C. Brashem-Stein, H. Voorhies, R.L. Manger, and I.D. Bernstein. 2010. Notch-mediated expansion of human cord blood progenitor cells capable of rapid myeloid reconstitution. *Nat. Med.* 16:232–236. http://dx.doi.org/10.1038/nm.2080

Ding, Y.Q., U. Marklund, W. Yuan, J. Yin, L. Wegman, J. Ericson, E. Deneris, R.L. Johnson, and Z.F. Chen. 2003. Lmx1b is essential for the development of serotonergic neurons. *Nat. Neurosci.* 6:933–938. http://dx.doi.org/10.1038/nn1104

Eijkelenboom, A., and B.M. Burgering. 2013. FOXOs: signalling integrators for homeostasis maintenance. *Nat. Rev. Mol. Cell Biol.* 14:83–97. http://dx.doi.org/10.1038/nrm3507

Fares, I., J. Chagraoui, Y. Gareau, S. Gingras, R. Ruel, N. Mayotte, E. Csaszar, D.J. Knapp, P. Miller, M. Ngom, et al. 2014. Pyrimidoindole derivatives are agonists of human hematopoietic stem cell self-renewal. *Science.* 345:1509–1512. http://dx.doi.org/10.1126/science.1256337

Fitch, S.R., G.M. Kimber, N.K. Wilson, A. Parker, B. Mirshekar-Syahkal, B. Göttgens, A. Medvinsky, E. Dzierzak, and K. Ottersbach. 2012. Signaling from the sympathetic nervous system regulates hematopoietic stem cell emergence during embryogenesis. *Cell Stem Cell.* 11:554–566. http://dx.doi.org/10.1016/j.stem.2012.07.002

Fonseca-Pereira, D., S. Arroz-Madeira, M. Rodrigues-Campos, I.A.M. Barbosa, R.G. Domingues, T. Bento, A.R.M. Almeida, H. Ribeiro, A.J. Potocnik, H. Enomoto, and H.Veiga-Fernandes. 2014. The neurotrophic factor receptor RET drives haematopoietic stem cell survival and function. *Nature.* 514:98–101. http://dx.doi.org/10.1038/nature13498

Fukumoto, T., I.P. Kema, and M. Levin. 2005. Serotonin signaling is a very early step in patterning of the left-right axis in chick and frog embryos. *Curr. Biol.* 15:794–803. http://dx.doi.org/10.1016/j.cub.2005.03.044

Ghosh, S., and C.K. Chan. 2016. Analysis of RNA-Seq data using TopHat and Cufflinks. *Methods Mol. Biol.* 1374:339–361. http://dx.doi.org/10.1007/978-1-4939-3167-5_18

Goessling, W., T.E. North, S. Loewer, A.M. Lord, S. Lee, C.L. Stoick-Cooper, G. Weidinger, M. Puder, G.Q. Daley, R.T. Moon, and L.I. Zon. 2009. Genetic interaction of PGE2 and Wnt signaling regulates developmental specification of stem cells and regeneration. *Cell.* 136:1136–1147. http://dx.doi.org/10.1016/j.cell.2009.01.015

Gratwohl, A., H. Baldomero, M. Aljurf, M.C. Pasquini, L.F. Bouzas, A. Yoshimi, J. Szer, J. Lipton, A. Schwendener, M. Gratwohl, et al. Worldwide Network of Blood and Marrow Transplantation. 2010. Hematopoietic stem cell transplantation: a global perspective. *JAMA.* 303:1617–1624. http://dx.doi.org/10.1001/jama.2010.491

Gutknecht, L., J. Waider, S. Kraft, C. Kriegebaum, B. Holtmann, A. Reif, A. Schmitt, and K.P. Lesch. 2008. Deficiency of brain 5-HT synthesis but serotonergic neuron formation in Tph2 knockout mice. *J Neural Transm (Vienna).* 115:1127–1132. http://dx.doi.org/10.1007/s00702-008-0096-6

Hannon, J., and D. Hoyer. 2008. Molecular biology of 5-HT receptors. *Behav. Brain Res.* 195:198–213. http://dx.doi.org/10.1016/j.bbr.2008.03.020

Hendricks, T.J., D.V. Fyodorov, L.J. Wegman, N.B. Lelutiu, E.A. Pehek, B. Yamamoto, J. Silver, E.J. Weeber, J.D. Sweatt, and E.S. Deneris. 2003. Pet-1 ETS gene plays a critical role in 5-HT neuron development and is required for normal anxiety-like and aggressive behavior. *Neuron.* 37:233–247. http://dx.doi.org/10.1016/S0896-6273(02)01167-4

Ichiyama, A., S. Nakamura, Y. Nishizuka, and O. Hayaishi. 1970. Enzymic studies on the biosynthesis of serotonin in mammalian brain. *J. Biol. Chem.* 245:1699–1709.

Katayama, Y., M. Battista, W.M. Kao, A. Hidalgo, A.J. Peired, S.A. Thomas, and P.S. Frenette. 2006. Signals from the sympathetic nervous system regulate hematopoietic stem cell egress from bone marrow. *Cell.* 124:407–421. http://dx.doi.org/10.1016/j.cell.2005.10.041

Kissa, K., and P. Herbomel. 2010. Blood stem cells emerge from aortic endothelium by a novel type of cell transition. *Nature.* 464:112–115. http://dx.doi.org/10.1038/nature08761

Koh, F.M., C.O. Lizama, P. Wong, J.S. Hawkins, A.C. Zovein, and M. Ramalho-Santos. 2015. Emergence of hematopoietic stem and progenitor cells involves a Chd1-dependent increase in total nascent transcription. *Proc. Natl. Acad. Sci. USA.* 112:E1734–E1743. http://dx.doi.org/10.1073/pnas.1424850112

Kriegebaum, C., N.N. Song, L. Gutknecht, Y. Huang, A. Schmitt, A. Reif, Y.Q. Ding, and K.P. Lesch. 2010. Brain-specific conditional and time-specific inducible Tph2 knockout mice possess normal serotonergic gene expression in the absence of serotonin during adult life. *Neurochem. Int.* 57:512–517. http://dx.doi.org/10.1016/j.neuint.2010.06.015

Kumaravelu, P., L. Hook, A.M. Morrison, J. Ure, S. Zhao, S. Zuyev, J. Ansell, and A. Medvinsky. 2002. Quantitative developmental anatomy of definitive haematopoietic stem cells/long-term repopulating units (HSC/RUs): role of the aorta-gonad-mesonephros (AGM) region and the yolk sac in colonisation of the mouse embryonic liver. *Development.* 129:4891–4899.

Kwan, W., M. Cortes, I. Frost, V. Esain, L.N. Theodore, S.Y. Liu, N. Budrow, W. Goessling, and T.E. North. 2016. The central nervous system regulates embryonic HSPC production via stress-responsive glucocorticoid receptor signaling. *Cell Stem Cell.* 19:370–382. http://dx.doi.org/10.1016/j.stem.2016.06.004

Li, Y., W. Zhong, D. Wang, Q. Feng, Z. Liu, J. Zhou, C. Jia, F. Hu, J. Zeng, Q. Guo, et al. 2016. Serotonin neurons in the dorsal raphe nucleus encode reward signals. *Nat. Commun.* 7:10503. http://dx.doi.org/10.1038/ncomms10503

Lillesaar, C., B. Tannhäuser, C. Stigloher, E. Kremmer, and L. Bally-Cuif. 2007. The serotonergic phenotype is acquired by converging genetic mechanisms within the zebrafish central nervous system. *Dev. Dyn.* 236:1072–1084. http://dx.doi.org/10.1002/dvdy.21095

Liu, Y., Y. Jiang, Y. Si, J.Y. Kim, Z.F. Chen, and Y. Rao. 2011. Molecular regulation of sexual preference revealed by genetic studies of 5-HT in the brains of male mice. *Nature.* 472:95–99. http://dx.doi.org/10.1038/nature09822

Liu, Z., J. Zhou, Y. Li, F. Hu, Y. Lu, M. Ma, Q. Feng, J.E. Zhang, D. Wang, J. Zeng, et al. 2014. Dorsal raphe neurons signal reward through 5-HT and glutamate. *Neuron.* 81:1360–1374. http://dx.doi.org/10.1016/j.neuron.2014.02.010

Lovenberg, W., E. Jequier, and A. Sjoerdsma. 1967. Tryptophan hydroxylation: measurement in pineal gland, brainstem, and carcinoid tumor. *Science.* 155:217–219. http://dx.doi.org/10.1126/science.155.3759.217

Lu, X., X. Li, Q. He, J. Gao, Y. Gao, B. Liu, and F. Liu. 2013. miR-142-3p regulates the formation and differentiation of hematopoietic stem cells in vertebrates. *Cell Res.* 23:1356–1368. http://dx.doi.org/10.1038/cr.2013.145

Méndez-Ferrer, S., D. Lucas, M. Battista, and P.S. Frenette. 2008. Haematopoietic stem cell release is regulated by circadian oscillations. *Nature.* 452:442–447. http://dx.doi.org/10.1038/nature06685

Moriya, Y., M. Itoh, S. Okuda, A.C. Yoshizawa, and M. Kanehisa. 2007. KAAS: an automatic genome annotation and pathway reconstruction server. *Nucleic Acids Res.* 35:W182–W185. http://dx.doi.org/10.1093/nar/gkm321

Mortazavi, A., B.A. Williams, K. McCue, L. Schaeffer, and B. Wold. 2008. Mapping and quantifying mammalian transcriptomes by RNA-Seq. *Nat. Methods.* 5:621–628. http://dx.doi.org/10.1038/nmeth.1226

Nichols, D.E., and C.D. Nichols. 2008. Serotonin receptors. *Chem. Rev.* 108:1614–1641. http://dx.doi.org/10.1021/cr078224o

North, T.E., W. Goessling, C.R. Walkley, C. Lengerke, K.R. Kopani, A.M. Lord, G.J. Weber, T.V. Bowman, I.H. Jang, T. Grosser, et al. 2007. Prostaglandin E2 regulates vertebrate haematopoietic stem cell homeostasis. *Nature.* 447:1007–1011. http://dx.doi.org/10.1038/nature05883

Orkin, S.H., and L.I. Zon. 2008. Hematopoiesis: an evolving paradigm for stem cell biology. *Cell.* 132:631–644. http://dx.doi.org/10.1016/j.cell.2008.01.025

Ortiz, J., and F. Artigas. 1992. Effects of monoamine uptake inhibitors on extracellular and platelet 5-hydroxytryptamine in rat blood: different effects of clomipramine and fluoxetine. *Br. J. Pharmacol.* 105:941–946. http://dx.doi.org/10.1111/j.1476-5381.1992.tb09082.x

Raghavendra, P.B., N. Pathak, and S.K. Manna. 2009. Novel role of thiadiazolidine derivatives in inducing cell death through Myc-Max, Akt, FKHR, and FasL pathway. *Biochem. Pharmacol.* 78:495–503. http://dx.doi.org/10.1016/j.bcp.2009.04.032

Rapport, M.M., A.A. Green, and I.H. Page. 1948. Serum vasoconstrictor, serotonin; isolation and characterization. *J. Biol. Chem.* 176:1243–1251.

Reisoli, E., S. De Lucchini, I. Nardi, and M. Ori. 2010. Serotonin 2B receptor signaling is required for craniofacial morphogenesis and jaw joint formation in *Xenopus*. *Development.* 137:2927–2937. http://dx.doi.org/10.1242/dev.041079

Rena, G., S. Guo, S.C. Cichy, T.G. Unterman, and P. Cohen. 1999. Phosphorylation of the transcription factor forkhead family member FKHR by protein kinase B. *J. Biol. Chem.* 274:17179–17183. http://dx.doi.org/10.1074/jbc.274.24.17179

Rentas, S., N.T. Holzapfel, M.S. Belew, G.A. Pratt, V. Voisin, B.T. Wilhelm, G.D. Bader, G.W. Yeo, and K.J. Hope. 2016. Musashi-2 attenuates AHR signalling to expand human haematopoietic stem cells. *Nature.* 532:508–511. http://dx.doi.org/10.1038/nature17665

Shukla, S., F. Rizvi, S. Raisuddin, and P. Kakkar. 2014. FoxO proteins' nuclear retention and BH3-only protein Bim induction evoke mitochondrial dysfunction-mediated apoptosis in berberine-treated HepG2 cells. *Free Radic. Biol. Med.* 76:185–199. http://dx.doi.org/10.1016/j.freeradbiomed.2014.07.039

Song, G., G. Ouyang, and S. Bao. 2005. The activation of Akt/PKB signaling pathway and cell survival. *J. Cell. Mol. Med.* 9:59–71. http://dx.doi.org/10.1111/j.1582-4934.2005.tb00337.x

Thambyrajah, R., M. Mazan, R. Patel, V. Moignard, M. Stefanska, E. Marinopoulou, Y. Li, C. Lancrin, T. Clapes, T. Möröy, et al. 2016. GFI1 proteins orchestrate the emergence of haematopoietic stem cells through recruitment of LSD1. *Nat. Cell Biol.* 18:21–32. http://dx.doi.org/10.1038/ncb3276

Wang, L., Z. Feng, X. Wang, X. Wang, and X. Zhang. 2010. DEGseq: an R package for identifying differentially expressed genes from RNA-seq data. *Bioinformatics.* 26:136–138. http://dx.doi.org/10.1093/bioinformatics/btp612

Wang, L., P. Zhang, Y. Wei, Y. Gao, R. Patient, and F. Liu. 2011. A blood flow-dependent *klf2a*-NO signaling cascade is required for stabilization of hematopoietic stem cell programming in zebrafish embryos. *Blood.* 118:4102–4110. http://dx.doi.org/10.1182/blood-2011-05-353235

Wang, L., T. Liu, L. Xu, Y. Gao, Y. Wei, C. Duan, G.Q. Chen, S. Lin, R. Patient, B. Zhang, et al. 2013. Fev regulates hematopoietic stem cell development via ERK signaling. *Blood.* 122:367–375. http://dx.doi.org/10.1182/blood-2012-10-462655

Wong, D.T., J.S. Horng, F.P. Bymaster, K.L. Hauser, and B.B. Molloy. 1974. A selective inhibitor of serotonin uptake: Lilly 110140, 3-(p-Trifluoromethylphenoxy)-n-methyl-3-phenylpropylamine. *Life Sci.* 15:471–479. http://dx.doi.org/10.1016/0024-3205(74)90345-2

Yang, M., K. Li, P.C. Ng, C.K. Chuen, T.K. Lau, Y.S. Cheng, Y.S. Liu, C.K. Li, P.M. Yuen, A.E. James, et al. 2007. Promoting effects of serotonin on hematopoiesis: ex vivo expansion of cord blood $CD34^+$ stem/progenitor cells, proliferation of bone marrow stromal cells, and antiapoptosis. *Stem Cells.* 25:1800–1806. http://dx.doi.org/10.1634/stemcells.2007-0048

Zhang, C., J. Lv, Q. He, S. Wang, Y. Gao, A. Meng, X. Yang, and F. Liu. 2014. Inhibition of endothelial ERK signalling by Smad1/5 is essential for haematopoietic stem cell emergence. *Nat. Commun.* 5:3431.

Zhang, P., Q. He, D. Chen, W. Liu, L. Wang, C. Zhang, D. Ma, W. Li, B. Liu, and F. Liu. 2015. G protein-coupled receptor 183 facilitates endothelial-to-hematopoietic transition via Notch1 inhibition. *Cell Res.* 25:1093–1107. http://dx.doi.org/10.1038/cr.2015.109

Zill, P., A. Büttner, W. Eisenmenger, J. Müller, H.J. Möller, and B. Bondy. 2009. Predominant expression of tryptophan hydroxylase 1 mRNA in the pituitary: a postmortem study in human brain. *Neuroscience.* 159:1274–1282. http://dx.doi.org/10.1016/j.neuroscience.2009.01.006

Zovein, A.C., J.J. Hofmann, M. Lynch, W.J. French, K.A. Turlo, Y. Yang, M.S. Becker, L. Zanetta, E. Dejana, J.C. Gasson, et al. 2008. Fate tracing reveals the endothelial origin of hematopoietic stem cells. *Cell Stem Cell.* 3:625–636. http://dx.doi.org/10.1016/j.stem.2008.09.018